cytosol to mitochondrial matrix via PiC may be a rate-limiting step for ATP production. However, precise detection of PiC and its significance in metabolism–secretion coupling in pancreatic β-cells has not been reported previously. In the present study, the role of PiC in metabolism–secretion coupling in pancreatic β-cells is evaluated using INS-1 cells manipulated to reduce PiC expression.

EXPERIMENTAL

Materials

ATP, ADP, poly-L-ornithine, DAPP (diadenosine pentaphosphate), Safranin O, FCCP (carbonyl cyanide *p*-trifluoromethoxyphenylhydrazone), ATP sulfurylase and Na_2MoO_4 were purchased from Sigma. Hepes, KCl, EGTA, sodium pyruvate, $MgSO_4$, NaH_2PO_4, $CaCl_2$, glucose, NaCl, $NaHCO_3$, $HClO_4$, Na_2CO_3, pyruvate kinase, BSA, KOH, potassium gluconate and KH_2PO_4 were purchased from Nacalai. 2-mercaptoethanol, penicillin, streptomycin and mouse monoclonal antibodies to the subunits of the mitochondrial respiratory chain complexes were purchased from Invitrogen. Luciferin-luciferase was purchased from Promega.

Cell culture

INS-1 (rat insulinoma) cells were cultured in RPMI 1640 medium containing 11.1 mM glucose (Invitrogen) supplemented with 10 % heat-inactivated fetal calf serum, 10 mM Hepes, 2 mM L-glutamine, 1 mM sodium pyruvate, 50 μM 2-mercaptoethanol, 100 IU/ml penicillin and 100 μg/ml streptomycin at 37 °C in a humidified atmosphere (5 % CO_2 and 95 % air). COS-7 (African green monkey kidney) cells were cultured in Dulbecco's modified Eagle's medium supplemented with 10 % heat-inactivated fetal calf serum, 100 IU/ml penicillin and 100 μg/ml streptomycin at 37 °C in a humidified atmosphere (5 % CO_2 and 95 % air).

siRNA transfection

Stealth™ siRNAs were synthesized by Invitrogen. The sequences of siRNAs specific for both rat PiC-A and PiC-B were: 5′-AAAUAUGCCCUUGUACUUCUGAGGG-3′ and 5′-CCCUCAGAAGUACAAGGGCAUAUUU-3′ designated as PiC siRNA1 and 5′-GAACACCUAUCUGUGGCGUACAUCA-3′ and 5′-UGAUGUACGCCACAGAUAGGUGUUC-3′ designated as PiC siRNA2. The sequences of control siRNAs were: 5′-ACCAACAACAGUUUGGGAAUAGGGA-3′ and 5′-UCCCUAUUCCCAAACUGUUGUUGGU-3′. Cultured INS-1 cells were trypsinized, suspended with RPMI 1640 medium without antibiotics, mixed with Opti-MEM (Invitrogen) containing siRNA and Lipofectamine™ 2000 (Invitrogen), plated on dishes or wells and then incubated at 37 °C in a CO_2 incubator. The final amounts of INS-1 cells, RPMI 1640, Opti-MEM, siRNA and Lipofectamine™ 2000 were 1×10^6 cells/ml, 75 % (v/v), 25 % (v/v), 80 nM and 0.3 % respectively. Medium was replaced with RPMI 1640 3–4 h after transfection. All experiments using siRNA-transfected INS-1 cells were performed 48 h after transfection unless otherwise noted.

Isolation of total RNA and quantitative RT (reverse transcription)–PCR

Total RNA was isolated from cardiac muscle, brain, skeletal muscle, kidney, liver and lung of Wistar rats using TRIzol® (Invitrogen) and from islets of Wistar rats and INS-1 cells using RNeasy mini kit (Qiagen). Animals were maintained and used in accordance with the Guidelines for Animal Experiments of Kyoto University. Islets were isolated by collagenase digestion [17]. cDNA was prepared by reverse transcriptase (Superscript II; Invitrogen) with an oligo(dT) primer. The rat sequences of forward and reverse primers to detect PiC-A, PiC-B, total PiC (PiC-A plus PiC-B) and β-actin (as an inner control) are shown in Table 1. AmpliTaq Gold (Applied Biosystems) was used as a DNA polymerase for RT–PCR. SYBR Green PCR Master Mix (Applied Biosystems) was prepared for the quantitative RT–PCR run. The thermal cycling conditions were denaturation at 95 °C for 10 min followed by 40 cycles at 95 °C for 30s and 60 °C for 30s.

Table 1 Primer sequences used in RT–PCR and quantitative RT–PCR

Name	Forward	Reverse
PiC-A	5′-AGCTGGTGCACGATGTGTCG-3′	5′-TTCCTCCGAGTCCACAGAGG-3′
PiC-B	5′-AGCTGGTGCACGATGTGTCG-3′	5′-CCACCAAAGCCACACAGTGC-3′
Total PiC (PiC-A+PiC-B)	5′-AGAGCAGCTGGTTGTGACAT-3′	5′-ACACCTCTAAAGCCAAGCCT-3′
β-actin	5′-CAATGAGCGGTTCCGATGCC-3′	5′-AATGCCTGGGTACATGGTGG-3′

Plasmid construction and transfection

The cDNA fragment of rat PiC-B was obtained from rat islets by RT–PCR and cloned into the pHMCA5 vector. pHMCA5-PiC-B was transfected into COS-7 and INS-1 cells using FuGENE™ 6 transfection reagent (Roche) and Lipofectamine™ 2000 respectively.

Immunoblot analysis

Rabbit antibody against the rat PiC peptide PPEM-PESLKKKLGLTE corresponding to C-terminal residues was originally raised. For immunoblotting, cells were washed with PBS containing protease inhibitor (Complete; Roche), suspended in 1 ml of PBS containing protease inhibitor and homogenized. Protein (50 μg per sample) was separated on a 15 % polyacrylamide gel and transferred to a nitrocellulose membrane. After blocking with TBS (Tris-buffered saline; 10 mM Tris/HCl and 100 mM NaCl, pH 7.5) containing 0.1 % Tween 20 and 5 % skimmed milk (blocking buffer) at room temperature (25 °C) for 2 h, blotted membranes were incubated overnight at 4 °C with anti-PiC antibody at 1:500 dilution, anti-DIC (dicarboxylate carrier) antibody (Novus Biologicals) at 1:100 dilution, mouse monoclonal anti-complex I (39 kDa subunit) antibody, anti-complex III (core II) antibody, anti-complex IV (subunit I) antibody or anti-complex V (subunit α) of mitochondrial respiratory chain antibody at 1:1000 dilution in blocking buffer, and subsequently with anti-rabbit (for PiC and DIC) or anti-mouse (for respiratory chain proteins) IgG horseradish peroxidase-conjugated secondary antibody (GE Healthcare) diluted 1:5000 at room temperature for 2 h prior to detection using ECL (GE Healthcare). In the same membrane, the process was repeated for β-actin at 1:1000 dilution of the antibody. Band intensities were quantified with Multi Gauge software (Fujifilm).

Insulin secretion

For insulin secretion assays, INS-1 cells cultured on 24-well plates coated with 0.001 % poly-L-ornithine were washed with KRBH (Krebs-Ringer bicarbonate Hepes buffer) composed of

140 mM NaCl, 3.6 mM KCl, 0.5 mM $MgSO_4$, 0.5 mM NaH_2PO_4, 1.5 mM $CaCl_2$, 2 mM $NaHCO_3$, 0.1 % BSA and 10 mM Hepes (pH 7.4) with 2 mM glucose, preincubated at 37 °C for 30 min in KRBH with 2 mM glucose, and then incubated at 37 °C for 30 min in KRBH with 2 mM glucose, 10 mM glucose or 2 mM glucose plus 30 mM KCl. Insulin concentrations were determined by RIA using rat insulin as a standard as previously described [17].

Adenine nucleotides

ATP and ADP contents were determined as previously described [18,19] with some modifications. Briefly, INS-1 cells were cultured, washed and preincubated as described above and incubated with KRBH with 2 mM glucose, 10 mM glucose or 2 mM glucose plus 30 mM KCl at 37 °C for 30 min. Incubation was stopped by the addition of $HClO_4$. The contents of wells were sonicated [three pulses of 3 s duration using a Handy Sonic UR-20P instrument (TOMY SEIKO) on ice] and transferred into glass tubes. The tubes were then centrifuged, and a fraction of the supernatant was neutralized with Hepes and Na_2CO_3. The ATP concentration was measured by luciferin-luciferase assay. After ATP in the neutralized extract was irreversibly converted to AMP with ATP sulfurylase in the presence of Na_2MoO_4, ADP in the reactant was converted to ATP with pyruvate kinase and was determined by luciferin-luciferase assay as the difference between the measurements with and without pyruvate kinase.

Intracellular calcium concentration ($[Ca^{2+}]_i$) and mitochondrial membrane potential ($\Delta\psi_m$) in living cells

INS-1 cells were seeded on to glass coverslips coated with 0.001 % poly-L-ornithine and cultured 48 h before measurements were made. For measurements of $[Ca^{2+}]_i$, cultured INS-1 cells were loaded with 5 μM Fura-PE3/AM (Calbiochem) at 37 °C for 90 min, placed in a heat-controlled chamber on the stage of an inverted microscope kept at 36 ± 1 °C, superfused with KRBH containing 2 mM glucose, and subsequently exposed to the buffer containing 10 mM glucose or 30 mM KCl. The cells were excited successively at 340 and 380 nm, and the fluorescence emitted at 510 nm was captured by CCD camera (Micro Max 5 MHz System, Roper Industries, Trenton, NJ). The images were analysed with the Meta Fluor image analyzing system (Universal Imaging). The 340 nm (F340) and 380 nm (F380) fluorescence signals were detected every 15 s, and ratios (F340/F380) were calculated. For $\Delta\psi_m$ measurements, the same protocol as above was used except that cultured cells were loaded with 10 μg/ml rhodamine 123 (Invitrogen) at 37 °C for 30 min and fluorescence excited at 490 nm and emitted at 530 nm every 20 s was monitored.

ATP production and $\Delta\psi_m$ in mitochondrial fraction

Measurement of ATP production from the mitochondrial fraction was performed as previously described [18] with minor modifications. Firstly, INS-1 cells were homogenized in solution A consisting of 50 mM Hepes, 100 mM KCl, 1.8 mM ATP, 1 mM EGTA, 2 mM $MgCl_2$ and 0.5 mg/ml BSA (electrophoretically homogeneous) with the pH adjusted to 7.00 at 37 °C with KOH. After precipitation of cell debris and nuclei by 800 *g* centrifugation for 3 min, the supernatant was centrifuged more rapidly (10000 *g* for 3 min) to obtain a pellet containing the mitochondrial fraction. The precipitation, diluted by 200 μl of solution A, was centrifuged again and rinsed three times in solution B, consisting of 20 mM Hepes, 1 mM EGTA, 12 mM NaCl, 0.3 mM $MgCl_2$, 130 mM potassium gluconate and 0.5 mg/ml BSA (electrophoretically homogeneous) with the pH adjusted to 7.10 with KOH. The mitochondrial fraction in 500 μl of solution B was kept on ice until use. To measure ATP production by oxidative phosphorylation, the reaction was started by adding mitochondrial suspension to prewarmed solution B (37 °C) containing mitochondrial substrates with or without respiratory chain inhibitors, 50 μM ADP, 1 μM DAPP and various levels of P_i. DAPP, a specific inhibitor of adenylate kinase, was used to measure ATP production by oxidative phosphorylation exclusively. After the reaction was stopped, the ATP concentration in the solutions was measured by adding luciferin-luciferase solution with a bioluminometer. ATP production was corrected by mitochondrial protein content. Measurement of $\Delta\psi_m$ was performed as previously described [20] with some modifications. Fluorescence was successively monitored using a spectrofluorophotometer (RF 5000; Shimadzu) with an excitation wavelength of 495 nm and emission at 586 nm, and with stirring solution B supplemented with 3 mM KH_2PO_4, 50 μM ADP and 2.5 μM Safranin O applied in a glass cuvette at 37 °C. Mitochondria, succinate and FCCP were added to the solution in this order and final concentrations were 50 μg/ml, 1 mM and 200 nM respectively.

Statistical analysis

The data are expressed as means ± S.E.M. Statistical significance was calculated by unpaired Student's *t* test. $P < 0.05$ was considered significant.

RESULTS

Expression of PiC mRNA in pancreatic β-cells

Tissue distribution of PiC was evaluated by RT–PCR (Figure 1A). PiC-B was expressed ubiquitously whereas PiC-A was expressed clearly in cardiac muscle and skeletal muscle as previously reported [13,14] and obscurely in rat islets and INS-1 cells. These results indicate that PiC-B was dominantly expressed in pancreatic β-cells.

Evaluation of anti-PiC antibody

The cell lysates of COS-7 cells transfected with pHMCA5-PiC or pHMCA5-null, INS-1 cells transfected with pHMCA5-null, intact INS-1 cells and rat islets were electrophoresed and immunoblotted using the anti-PiC antibody. As shown in Figure 1(B), the band at ~30 kDa, which was not detected in COS-7 cells transfected with pHMCA5-null, was detected in COS-7 cells transfected with pHMCA5-PiC, INS-1 cells transfected with pHMCA5-null, intact INS-1 cells and rat islets. This observation is consistent with a previous report that rat PiC was detected at ~30 kDa by an antibody originally raised using the C-terminal amino acids as the antigen peptide [21].

Silencing effects of PiC siRNAs on INS-1 cells

Quantitative RT–PCR assays using primers for total PiC (PiC-A plus PiC-B, Table 1) and immunoblotting using anti-PiC antibody revealed ~70 % reduction of PiC mRNA expression and ~40 % reduction of the protein expression in INS-1 cells 48 h after both PiC siRNA1 and 2 transfection respectively (Figures 1C and 1D). Time-dependent reduction of PiC protein expression (~25 %, ~40 % and ~50 % reduction at 24 h, 48 h and 72 h after siRNA1 and 2 transfection) implies long half-life of PiC, which causes low efficacy of suppression (Figure 1D). Transfection of control siRNA did not affect the expression of PiC in INS-1 cells at both mRNA and protein levels. Protein expressions of DIC,

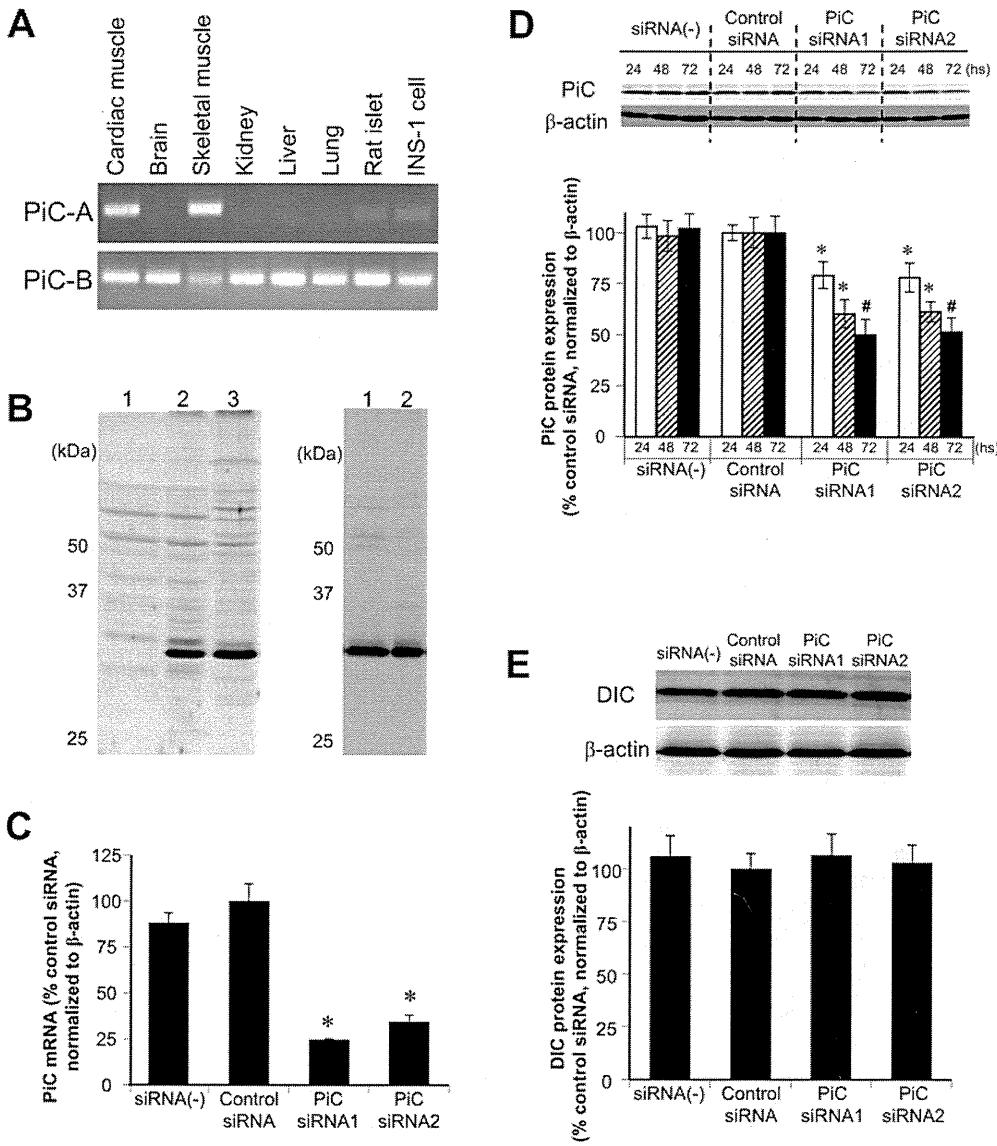

Figure 1 Detection of rat PiC and silencing effects of PiC siRNAs on INS-1 cells

(**A**) RT–PCR detection of PiC mRNA expression in various rat tissues and INS-1 cells. PiC mRNA expressions in cardiac muscle, brain, skeletal muscle, kidney, liver, lung and islets of Wistar rat and INS-1 cells were evaluated with RT–PCR using primers of specific sequences for PiC-A and PiC-B. Product sizes are 141 bp for PiC-A and 136 bp for PiC-B. (**B**) Evaluation of anti-PiC antibody by immunoblot analysis. Left panel: whole cell lysates from COS-7 cells transfected with pHMCA5-null (lane 1), COS-7 cells transfected with pHMCA5-PiC (lane 2) and INS-1 cells transfected with pHMCA5-null (lane 3) were electrophoresed and immunoblotted with anti-PiC antibody. Right panel: whole cell lysates from INS-1 cells (lane 1) and rat islets (lane 2) were electrophoresed and immunoblotted with anti-PiC antibody. Molecular mass in kDa is given on the left-hand side of each panel. (**C**) Effects of transfection of PiC siRNAs on the expression of PiC mRNA was evaluated with quantitative RT–PCR using a pair of primers recognizing both PiC-A and PiC-B (total PiC). Data were normalized using β-actin mRNA. $n = 3$ in each group. $^*P < 0.01$ compared with control siRNA. (**D**) Immunoblot analysis of PiC expression revealed that PiC siRNAs reduced PiC expression in INS-1 cells. Time (h) after siRNA transfection is indicated. Data were normalized by the expression of β-actin. $n = 4$ in each bar. $^*P < 0.05$ and $\#P < 0.01$ compared with control siRNA. (**E**) Effects of PiC silencing on expression of DIC. Whole INS-1 cell lysate was electrophoresed and immunoblotted using antibodies against DIC. Quantification data were obtained from four independent experiments and normalized with β-actin levels.

another P_i carrier, were not affected by siRNA1 and 2 transfection (Figure 1E).

Effects of PiC down-regulation on glucose- and depolarization-stimulated insulin secretion

Down-regulation of PiC decreased GSIS (10 mM glucose) in INS-1 cells, as shown in Figure 2. A reduction in GSIS of 61 % by PiC siRNA1 and 47 % by PiC siRNA2 was observed. K^+ (30 mM)-stimulated insulin secretion was also reduced: the reduction was 27 % by PiC siRNA1 and 23 % by PiC siRNA2, which were milder than those of GSIS (Figure 2). Insulin secretion in the basal glucose state (2 mM) was not affected by PiC siRNA1, but was slightly increased by PiC siRNA2. Transfection of control siRNA did not affect GSIS in INS-1 cells.

Effects of PiC down-regulation on adenine nucleotides

Down-regulation of PiC increased ADP and decreased the ATP:ADP ratio, whereas it did not significantly affect ATP in

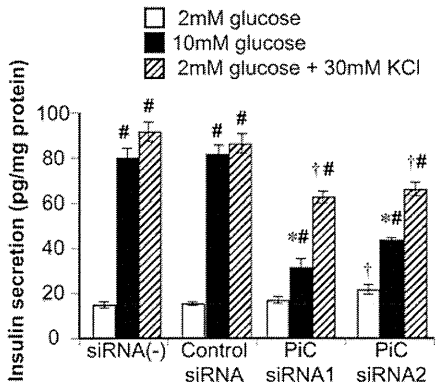

Figure 2 Effects of PiC down-regulation on glucose- or KCl-stimulated insulin secretion

INS-1 cells were incubated for 30 min with 2 mM glucose, 10 mM glucose or 2 mM glucose and 30 mM K^+, and insulin secretion was measured. Data were obtained from six independent experiments normalized by protein concentration. Error bars are means ± S.E.M. $*P < 0.01$ and $\dagger P < 0.05$ compared with control siRNA at the corresponding condition. $\#P < 0.01$ compared with corresponding 2 mM glucose.

the presence of 10 mM glucose in INS-1 cells (Table 2A). ATP, ADP and the ATP:ADP ratio at 2 mM glucose was not altered by silencing PiC (Tables 2A and 2B). Depolarization evoked by 30 mM K^+ in the presence of 2 mM glucose decreased the ATP:ADP ratio in both control and PiC down-regulated cells, whereas suppression of the ATP:ADP ratio was lower in PiC down-regulated cells compared with control cells (Table 2B).

Effects of PiC down-regulation on $[Ca^{2+}]_i$ and $\Delta\psi_m$ in living cells

Fluorescence signals of Fura-PE3 revealed that elevation of $[Ca^{2+}]_i$ in response to a stimulating level of 10 mM glucose was decreased and delayed by PiC down-regulation compared with that in control (Figure 3A). Average values calculated using the data from Figure 3(A) also indicate that PiC siRNA reduced the mean $[Ca^{2+}]_i$ at 10 mM glucose (PiC siRNA1, 0.864 ± 0.004 compared with control siRNA, 0.896 ± 0.003; $P < 0.01$) whereas there was no significant change at basal (2 mM) glucose (PiC siRNA1, 0.846 ± 0.004; control siRNA, 0.857 ± 0.003), as shown in Figure 3(B). Elevation of $[Ca^{2+}]_i$ in response to 30 mM K^+ was slightly decreased by PiC siRNA1 (average value of Fura-PE3 fluorescence ratio was 0.968 ± 0.005, compared with a control siRNA ratio of 0.991 ± 0.005, $P < 0.01$) without affecting basal value (control siRNA, 0.857 ± 0.006; siRNA1, 0.854 ± 0.004) as shown in Figures 3(C) and 3(D). Fluorescence measurement using rhodamine 123 demonstrated that the mitochondrial membrane in INS-1 cells was hyperpolarized by raising glucose from 2 to 10 mM and prominently depolarized by FCCP, and that PiC down-regulation did not affect glucose-induced hyperpolarization and total depolarization after FCCP exposure of $\Delta\psi_m$ throughout the measurement (Figure 3E).

Effects of PiC down-regulation on ATP production and $\Delta\psi_m$ in mitochondrial fraction

ATP production by mitochondria from INS-1 cells transfected with control or PiC siRNAs in the presence of 1 mM succinate and various concentrations of P_i ($[P_i]$) is shown in Figure 4(A). PiC down-regulation decreased mitochondrial ATP production by 50–60 % at $[P_i]$ ranging from 0.001 to 10 mM. ATP production in all groups reached maximum rates above ~3 mM of $[P_i]$, which indicates that the PiC amount regulates the maximal rate of mitochondrial ATP production. On the other hand, K_m values of $[P_i]$ for ATP production were similar (~0.05 mM). Mitochondrial ATP production in the presence of various mitochondrial substrates and inhibitors of the respiratory chain is shown in Table 3. ATP production in the presence of succinate was completely inhibited by antimycin A, a complex III inhibitor, in both control and PiC down-regulated INS-1 cells. PiC siRNAs decreased ATP production in the presence of pyruvate and malate by 42–58 %, succinate plus rotenone by 46–62 % and TMPD (*N*,*N*,*N*′,*N*′-tetramethyl-*p*-phenylenediamine) plus ascorbate by 61–62 %, showing that ATP production by electrons rendered at complex I, complex II and complex IV is suppressed to a similar degree. In spite of significant down-regulation of ATP production, PiC down-regulation did not affect $\Delta\psi_m$ of isolated mitochondria measured with Safranin O in the presence of succinate (Figure 4B).

Effects of PiC down-regulation on expression of mitochondrial respiratory chain proteins

Immunoblotting using lysates of whole INS-1 cells revealed that transfection of PiC siRNAs did not change the expression of complex I, III, IV or V of mitochondrial respiratory chain proteins (Figure 5).

DISCUSSION

In the present study, the mitochondrial phosphate carrier (PiC) was revealed to play an important role in metabolism–secretion coupling of pancreatic β-cells by using INS-1 cells and PiC siRNA. PiC down-regulation brings about reduction in mitochondrial ATP production by mitochondrial fuels, resulting in reduced glucose-induced $[Ca^{2+}]_i$ elevation and impaired GSIS.

In pancreatic β-cells, ATP increase is slight and ADP decrease is prominent via an increase in glucose levels beyond the triggering level of insulin secretion. In addition, the ATP/ADP ratio is well-correlated with GSIS rather than the absolute value of ATP [22,23]. PiC down-regulation decreased the ATP/ADP ratio in the presence of high glucose, which causes insufficient closure of K_{ATP} channels, a decrease in $[Ca^{2+}]_i$ elevation by glucose (Figures 3A and 3B), and suppression of GSIS (Figure 2).

Insulin secretion at 10 mM glucose was similar to that at 30 mM K^+ and 2 mM glucose in the control samples. In contrast, in PiC down-regulated INS-1 cells, GSIS is lower than depolarization-induced insulin secretion, which suggests specific effects of PiC on metabolism–secretion coupling (Figure 2). However, ~25 % suppression of depolarization-induced insulin secretion, which is modest compared with GSIS, was observed in PiC down-regulated INS-1 cells. Measurements revealed that $[Ca^{2+}]_i$ in the presence of 2 mM glucose and 30 mM K^+ was reduced by PiC down-regulation (Figures 3C and 3D), which plays a role in reduced depolarization-induced insulin secretion by PiC down-regulation. Depolarization reduced the ATP/ADP ratio in the presence of a basal level of glucose in control samples, which accords with a previous study where an increase in $[Ca^{2+}]_i$ causes a larger consumption than production of ATP [24] (Table 2B). The ATP/ADP ratio was also reduced by depolarization at 2 mM glucose in PiC down-regulated INS-1 cells, although the suppression was lower than that in control samples, which may reflect a smaller elevation of $[Ca^{2+}]_i$ than in the control. In addition, in contrast with a significant suppression of the ATP/ADP ratio at high glucose concentrations by PiC down-regulation, in the presence of a basal

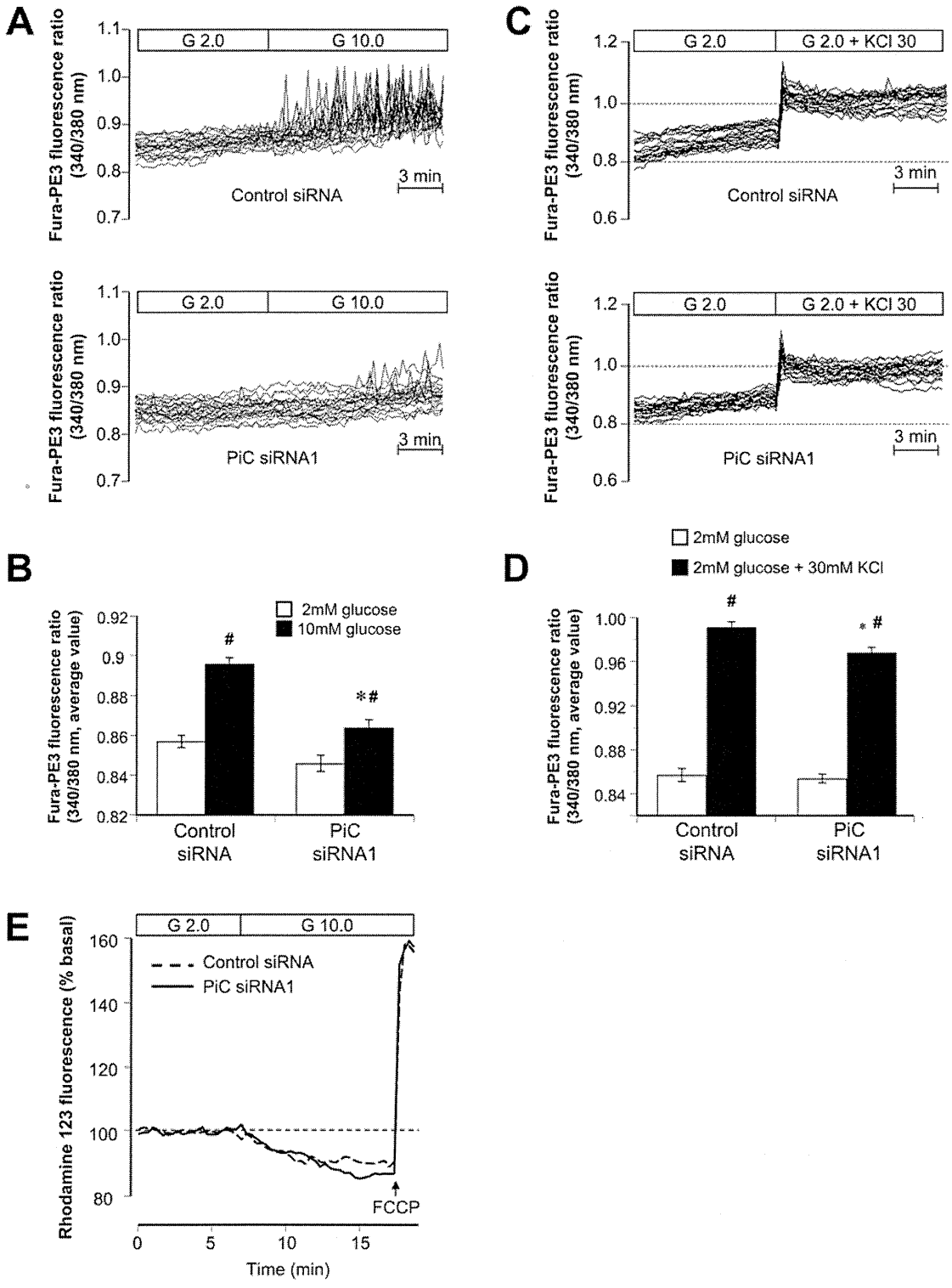

Figure 3 Effects of PiC down-regulation on $[Ca^{2+}]_i$ and $\Delta\psi_m$ in living cells

(**A**) $[Ca^{2+}]_i$ elevation and oscillation induced by raising glucose (G) from 2 to 10 mM were monitored in INS-1 cells transfected with PiC siRNA. Traces of Fura-PE3 fluorescence ratio (340/380 nm) were obtained from 20 cells of each group. (**B**) Average values calculated from the data from (**A**). $*P < 0.01$ compared with control siRNA at 10 mM glucose. $\#P < 0.01$ compared with corresponding 2 mM glucose. (**C**) $[Ca^{2+}]_i$ elevation induced by 30 mM KCl was monitored in INS-1 cells transfected with PiC siRNA. Traces of Fura-PE3 fluorescence ratio (340/380 nm) were obtained from 20 cells of each group. (**D**) Average values calculated from the data from (**C**). $*P < 0.05$ compared with control siRNA at 30 mM KCl. $\#P < 0.01$ compared with corresponding 2 mM glucose. (**E**) $\Delta\psi_m$ monitored by rhodamine 123 fluorescence in INS-1 cells. Data were corrected with the average values of fluorescence under basal glucose (2 mM) conditions. $n = 10$. Error bars are means±S.E.M.

Table 2 Effects of PiC down-regulation on adenine nucleotides

(A)

	Control siRNA		PiC siRNA1		PiC siRNA2	
Glucose (mM)	2	10	2	10	2	10
ATP (nmol/mg protein)	65.2 ± 3.8	77.4 ± 3.8*	64.4 ± 1.0	71.8 ± 3.3*	66.2 ± 1.7	80.0 ± 5.5*
ADP (nmol/mg protein)	10.2 ± 0.6	3.9 ± 0.4†	10.6 ± 0.6	6.4 ± 0.9*‡	9.7 ± 0.6	6.1 ± 1.2*‡
ATP/ADP	6.5 ± 0.6	20.5 ± 2.0†	6.1 ± 0.4	12.0 ± 1.7*‡	6.9 ± 0.5	13.9 ± 1.4*‡

(B)

	Control siRNA			PiC siRNA1	
Glucose (mM)	2	2	2	2	2
K^+ (mM)	3.6	30	3.6	3.6	30
Antimycin A (μM)	0	0	1	0	0
ATP (nmol/mg protein)	65.5 ± 3.4	48.6 ± 1.9*	2.5 ± 0.1†	64.4 ± 4.7	61.2 ± 1.8‡
ADP (nmol/mg protein)	10.1 ± 0.1	11.2 ± 0.2*	10.5 ± 0.1*	9.9 ± 0.2	10.5 ± 0.3*‡
ATP/ADP	6.5 ± 0.3	4.4 ± 0.2†	0.2 ± 0.0†	6.5 ± 0.5	5.8 ± 0.2*§

*$P < 0.05$ and †$P < 0.01$ compared with basal condition (2 mM glucose). ‡$P < 0.05$ and §$P < 0.01$ compared with control siRNA. Data were obtained from four independent experiments.

Table 3 Silencing effects of PiC siRNAs on ATP production from mitochondrial fraction of INS-1 cells

	Mitochondrial ATP production (μmol/10 min per mg of protein)		
Experimental conditions	Control siRNA	PiC siRNA1	PiC siRNA2
1 mM succinate	1.28 ± 0.02	0.61 ± 0.02*	0.46 ± 0.01*
1 mM succinate + 1 μM rotenone	1.03 ± 0.09	0.56 ± 0.03*	0.39 ± 0.01*
1 mM succinate + 1 μM antimycin A	0.03 ± 0.01	0.00 ± 0.01	0.00 ± 0.01
1 mM pyruvate + 1 mM malate	0.41 ± 0.03	0.24 ± 0.01*	0.17 ± 0.00*
0.5 mM TMPD + 2 mM ascorbate	3.43 ± 0.09	1.33 ± 0.03*	1.27 ± 0.01*

*$P < 0.01$ compared with control siRNA. Data were obtained from three independent experiments.

level of glucose, PiC down-regulation did not affect the ATP/ADP ratio in INS-1 cells. An incomplete compensatory effect derived from PiC down-regulation, which is valid in a basal supply of substrate to mitochondria but deteriorates in an accelerated supply at high glucose, might save ATP consumption and maintain the basal ratio of ATP/ADP.

PiC, which is required for mitochondrial ATP production, has two isoforms. PiC-A is expressed in skeletal and cardiac muscle whereas PiC-B is expressed ubiquitously. AAC (ATP/ADP carrier), which is also required for mitochondrial ATP production, has isoforms including AAC1 (SLC25A4), AAC2 (SLC25A5) and AAC3 (SLC25A6). Interestingly, these isoforms, except AAC2, expression of which is absent or scarce in most tissues, distribute similarly to the PiC isoforms: AAC1 is expressed in skeletal and cardiac muscle, and AAC3 is expressed ubiquitously. These distributions imply that ubiquitously-expressed PiC-B and AAC3 may meet stable energy requirement, and PiC-A and AAC1, which are expressed exclusively in muscle, meet higher and prompt energy demands for muscle contraction. In the present study, we demonstrate that PiC-B is the dominant isoform of PiC whereas PiC-A is scarcely expressed in INS-1 cells and rat islets (Figure 1A), which may reflect less prompt energy demand in β-cells compared with that in muscles.

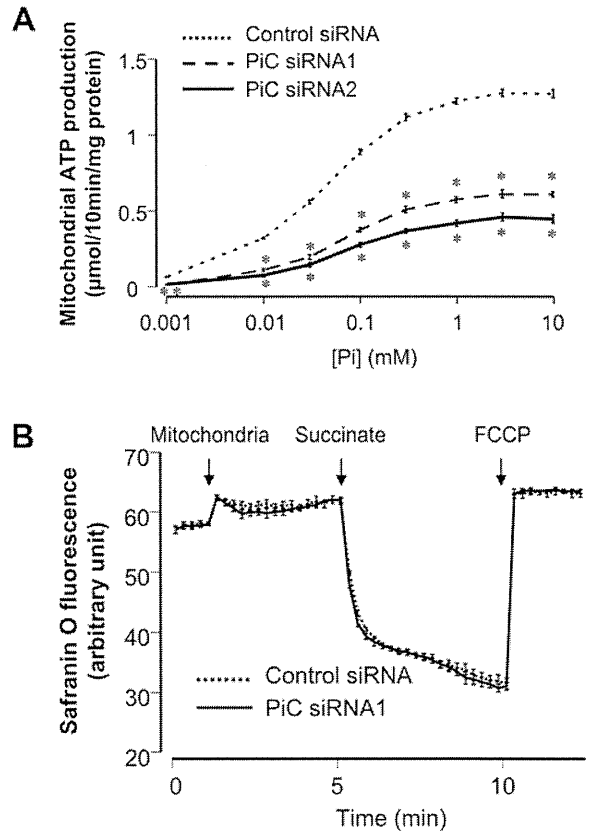

Figure 4 Effects of PiC down-regulation on ATP production and $\Delta\psi_m$ in mitochondrial fraction isolated from INS-1 cells

(**A**) Effects of PiC down-regulation on mitochondrial ATP production at various phosphate concentrations. ATP production was evaluated in mitochondria isolated from INS-1 cells in the presence of 50 μM ADP, 1 μM DAPP and 1 mM succinate with various concentrations of P_i indicated in the Figure. $n = 3$ in each plot. *$P < 0.01$ compared with control siRNA. (**B**) $\Delta\psi_m$ monitored by Safranin O fluorescence. Mitochondria (50 μg/ml), succinate (1 mM) and FCCP (200 nM) were added to the solution containing Safranin O at the points indicated with arrows. $n = 4$ in each group.

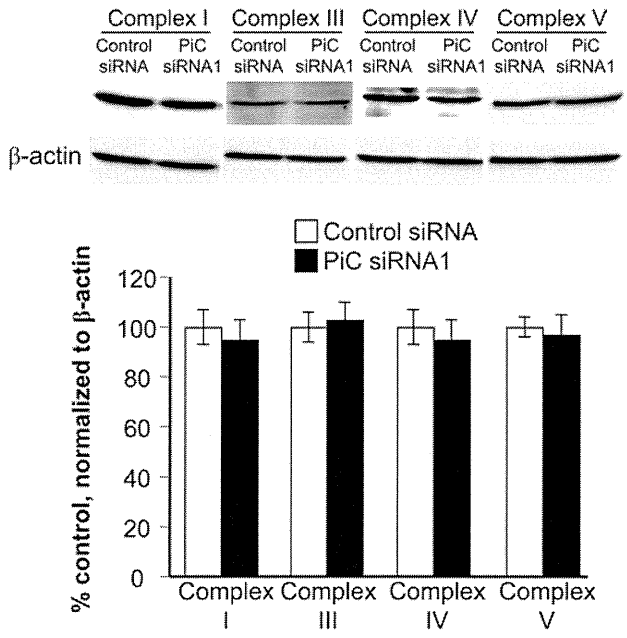

Figure 5 Effects of PiC silencing on expression of mitochondrial respiratory chain proteins

Lysates of whole INS-1 cells were electrophoresed and immunoblotted using antibodies against complex I, III, IV and V. Quantification data were obtained from four independent experiments and normalized with β-actin levels. Error bars are means±S.E.M.

Mitochondrial ATP is produced by complex V (ATP synthase), which is driven by protonmotive force generated by proton extrusion during transport of high-energy electrons in the respiratory chain. In the present study, mitochondrial ATP production in the presence of mitochondrial fuel increased according to the raised extramitochondrial phosphate concentration ($[P_i]_c$), and reached maximum rate above ~3 mM of $[P_i]_c$, which was decreased by 50–60 % without affecting the K_m value of $[P_i]_c$ for ATP production by ~40 % reduction in PiC protein. The physiological intracellular $[P_i]$ in heart determined by methods including ^{31}P NMR is ~1 mM at rest and increases to ~10 mM depending on the metabolic state [25–27]. Levels of P_i in islets are ~20 mmol/kg of dry weight tissue [28], which corresponds to ~10 mM by conversion [29]. Taken together, the rate of mitochondrial ATP production might be barely affected by a physiological change of $[P_i]_c$ but be evidently affected by alteration of the amount of PiC protein. In addition, reduction in ATP production by down-regulation of PiC also suggests that compensatory supply of P_i to mitochondria by other mitochondrial phosphate carriers including DIC (SLC25A10) [30,31] does not occur, which is supported by no apparent effect of PiC down-regulation on DIC expression (Figure 1E). These results accord with the first description that PiC dysfunction impairs the synthesis of ATP [15].

Intramitochondrial P_i is thought to affect oxidative phosphorylation at multiple sites [16]. To find specific defective sites in the respiratory chain in PiC down-regulated INS-1 cells, mitochondrial ATP production was examined in the presence of various substrates and inhibitors. Pyruvate and malate, which are metabolized in mitochondria to generate NADH, render electrons at complex I. In the presence of rotenone, a complex I inhibitor, succinate renders electrons directly to complex II via $FADH_2$. TMPD is an artificial electron donor that can transfer electrons to cytochrome *c*. TMPD reduced by ascorbate renders electrons to cytochrome *c*, which transfers electrons to complex IV. Reduction of ATP production by down-regulation of PiC in the presence of pyruvate plus malate, succinate plus rotenone and TMPD plus ascorbate were all suppressed similarly by 50–60 % (Table 3). These results indicate that reduction in ATP production by down-regulation of PiC may well be derived from a defective site downstream of complex IV and that a defective site upstream of complex IV, if present, does not play a prominent role. Moreover, immunoblotting revealed that expressions of respiratory chain proteins including complex I, III, IV and V were not affected by PiC silencing. Considered together, silencing of PiC seems to suppress mitochondrial ATP production not by affecting mitochondrial biogenesis, but by restricting P_i supply to complex V.

Inhibition of complex V by oligomycin reduces ATP production with hyperpolarization of $\Delta\psi_m$ [32,33], which may be derived from the fact that complex V is a protonophore and its inhibition affects electrogenic H^+ influx to mitochondria specifically and directly affects $\Delta\psi_m$. In contrast, PiC is electroneutral due to symport of H^+ and negatively charged P_i or antiport of OH^- and negatively charged P_i and does not directly affect $\Delta\psi_m$. ATP generation in complex V is driven by protonmotive force (Δp), which has two components: electrical membrane potential ($\Delta\psi_m$) and the difference between the cytosolic and matrix pH (ΔpH) [34,35]. P_i plays regulatory roles in oxidative phosphorylation by affecting Δp. An increase in $[P_i]_c$ reduces ΔpH [34,36–38] due to an increase in co-transport of P_i and protons from cytosol into mitochondrial matrix through PiC. On the other hand, $\Delta\psi_m$ is increased by an increase in $[P_i]_c$ of less than ~2 mM, but reaches a plateau at $[P_i]_c$ above ~2 mM [16,34,38]. Increases in $\Delta\psi_m$ owing to increases in $[P_i]_c$ is not fully elucidated, but some explanations are proposed. An electroneutral influx of protons (H^+) accompanying negatively charged substrates such as P_i does not directly affect $\Delta\psi_m$ but produces a reduction in ΔpH that promotes proton extrusion by the respiratory chain to maintain Δp and eventually increases $\Delta\psi_m$ [35]. Bose et al. [16] provided another explanation: an increase in the influx of P_i activates intramitochondrial NADH production and NADH supply to complex I and also promotes the ability to generate Δp by improving the coupling of electron transport between cytochrome *b* and cytochrome *c*, which eventually increases $\Delta\psi_m$. Interestingly, in the present study, ~40 % reduction in the protein level of PiC did not affect glucose-induced hyperpolarization of the mitochondrial inner membrane in spite of a reduction in ATP production. It is possible that the reduction in P_i influx by down-regulation of PiC in the present study is within a range of P_i influx which does not affect $\Delta\psi_m$ as with higher $[P_i]_c$. In addition, our results were derived from sustained down-regulation of P_i influx to mitochondria, as experiments were performed 48 h after transfection of PiC siRNA in contrast with the acute alteration of P_i influx by manipulation of $[P_i]_c$ in previous studies, which may permit adaptation of $\Delta\psi_m$ to maintain Δp.

It has been generally reported that the contribution of $\Delta\psi_m$ to Δp is 80–85 % [34,35,37–45] or more [16] and that of ΔpH is relatively small, which indicates that the alteration in Δp by down-regulation of PiC in the present study is small considering the non-detectable affect on $\Delta\psi_m$. Therefore the supply of P_i to complex V may well be a critical rate-limiting step for ATP production independent of Δp. The results in the present study demonstrate the critical role of P_i influx to mitochondria in ATP production and metabolism–secretion coupling in pancreatic β-cells.

AUTHOR CONTRIBUTION

Yuichi Nishi researched data, contributed to the discussion, wrote the manuscript and revised/edited the manuscript. Shimpei Fujimoto contributed to the discussion, wrote the manuscript and revised/edited the manuscript. Mayumi Sasaki, Eri Mukai, Hiroki Sato, Yuichi Sato, Yumiko Tahara and Yasuhiko Nakamura researched data. Nobuya Inagaki contributed to the discussion and revised/edited the manuscript.

ACKNOWLEDGEMENTS

We greatly appreciate the gifts of INS-1 cells from Dr Nobuo Sekine (Tokyo Kosei Nenkin Hospital, Tokyo, Japan) and pHMCA5 vector from Dr Hiroyuki Mizuguchi (National Institute of Biomedical Innovation, Ibaraki, Japan). We thank Mr Shinsaku Akagi, Mr Takuro Yamaguchi, Ms Chiyo Kotake and Ms Sara Yasui for technical assistance and Mr Eiji Yoshihara for helpful advice on siRNA transfection.

FUNDING

This study was supported by a Research Grant on Nanotechnical Medicine from the Ministry of Health, Labour, and Welfare of Japan, Scientific Research Grants, a grant from Innovation Cluster Kansai project of the Ministry of Education, Culture, Sports, Science and Technology of Japan, and a grant from CREST (Core Research for Evolutional Science and Technology) of Japan Science and Technology Cooperation.

REFERENCES

1 Maechler, P. and Wollheim, C. B. (2001) Mitochondrial function in normal and diabetic β-cells. Nature **414**, 807–812
2 Kennedy, E. D., Maechler, P. and Wollheim, C. B. (1998) Effects of depletion of mitochondrial DNA in metabolism secretion coupling in INS-1 cells. Diabetes **47**, 374–380
3 Tsuruzoe, K., Araki, E., Furukawa, N., Shirotani, T., Matsumoto, K., Kaneko, K., Motoshima, H., Yoshizato, K., Shirakami, A., Kishikawa, H. et al. (1998) Creation and characterization of a mitochondrial DNA-depleted pancreatic β-cell line: impaired insulin secretion induced by glucose, leucine, and sulfonylureas. Diabetes **47**, 621–631
4 Palmieri, F. (2004) The mitochondrial transporter family (SLC25): physiological and pathological implications. Pflugers Arch. **447**, 689–709
5 Rubi, B., del Arco, A., Bartley, C., Satrustegui, J. and Maechler, P. (2004) The malate-aspartate NADH shuttle member Aralar1 determines glucose metabolic fate, mitochondrial activity, and insulin secretion in beta cells. J. Biol. Chem. **279**, 55659–55666
6 Casimir, M., Rubi, B., Frigerio, F., Chaffard, G. and Maechler, P. (2009) Silencing of the mitochondrial NADH shuttle component aspartate-glutamate carrier AGC1/Aralar1 in INS-1E cells and rat islets. Biochem. J. **424**, 459–466
7 Chan, C. B., MacDonald, P. E., Saleh, M. C., Johns, D. C., Marban, E. and Wheeler, M. B. (1999) Overexpression of uncoupling protein 2 inhibits glucose-stimulated insulin secretion from rat islets. Diabetes **48**, 1482–1486
8 Zhang, C. Y., Baffy, G., Perret, P., Krauss, S., Peroni, O., Grujic, D., Hagen, T., Vidal-Puig, A. J., Boss, O., Kim, Y. B. et al. (2001) Uncoupling protein-2 negatively regulates insulin secretion and is a major link between obesity, β cell dysfunction, and type 2 diabetes. Cell **105**, 745–755
9 Odegaard, M. L., Joseph, J. W., Jensen, M. V., Lu, D., Ilkayeva, O., Ronnebaum, S. M., Becker, T. C. and Newgard, C. B. (2010) The mitochondrial 2-oxoglutarate carrier is part of a metabolic pathway that mediates glucose- and glutamine-stimulated insulin secretion. J. Biol. Chem. **285**, 16530–16537
10 Joseph, J. W., Jensen, M. V., Ilkayeva, O., Palmieri, F., Alarcon, C., Rhodes, C. J. and Newgard, C. B. (2006) The mitochondrial citrate/isocitrate carrier plays a regulatory role in glucose-stimulated insulin secretion. J. Biol. Chem. **281**, 35624–35632
11 Casimir, M., Lasorsa, F. M., Rubi, B., Caille, D., Palmieri, F., Meda, P. and Maechler, P. (2009) Mitochondrial glutamate carrier GC1 as a newly identified player in the control of glucose-stimulated insulin secretion. J. Biol. Chem. **284**, 25004–25014
12 Dolce, V., Iacobazzi, V., Palmieri, F. and Walker, J. E. (1994) The sequences of human and bovine genes of the phosphate carrier from mitochondria contain evidence of alternatively spliced forms. J. Biol. Chem. **269**, 10451–10460
13 Fiermonte, G., Dolce, V. and Palmieri, F. (1998) Expression in *Escherichia coli*, functional characterization, and tissue distribution of isoforms A and B of the phosphate carrier from bovine mitochondria. J. Biol. Chem. **273**, 22782–22787
14 Dolce, V., Fiermonte, G. and Palmieri, F. (1996) Tissue-specific expression of the two isoforms of the mitochondrial phosphate carrier in bovine tissues. FEBS Lett. **399**, 95–98
15 Mayr, J. A., Merkel, O., Kohlwein, S. D., Gebhardt, B. R., Böhles, H., Fötschl, U., Koch, J., Jaksch, M., Lochmüller, H. and Horváth, R. et al. (2007) Mitochondrial phosphate-carrier deficiency: a novel disorder of oxidative phosphorylation. Am. J. Hum. Genet. **80**, 478–484
16 Bose, S., French, S., Evans, F. J., Joubert, F. and Balaban, R. S. (2003) Metabolic network control of oxidative phosphorylation: multiple roles of inorganic phosphate. J. Biol. Chem. **278**, 39155–39165
17 Fujimoto, S., Ishida, H., Kato, S., Okamoto, Y., Tsuji, K., Mizuno, N., Ueda, S., Mukai, E. and Seino, Y. (1998) The novel insulinotropic mechanism of pimobendan: direct enhancement of the exocytotic process of insulin secretory granules by increased Ca^{2+} sensitivity in β-cells. Endocrinology **139**, 1133–1140
18 Takehiro, M., Fujimoto, S., Shimodahira, M., Shimono, D., Mukai, E., Nabe, K., Radu, R. G., Kominato, R., Aramaki, Y., Seino, Y. and Yamada, Y. (2005) Chronic exposure to β-hydroxybutyrate inhibits glucose-induced insulin release from pancreatic islets by decreasing NADH contents. Am. J. Physiol. **288**, E372–E380
19 Schultz, V., Sussman, I., Bokvist, K. and Tornheim, K. (1993) Bioluminometric assay of ADP and ATP at high ATP/ADP ratios: assay of ADP after enzymatic removal of ATP. Anal. Biochem. **215**, 302–304
20 Votyakova, T. V. and Reynolds, I. J. (2001) $\Delta\psi_m$-Dependent and -independent production of reactive oxygen species by rat brain mitochondria. J. Neurochem. **79**, 266–277
21 Leung, A. W., Varanyuwatana, P. and Halestrap, A. P. (2008) The mitochondrial phosphate carrier interacts with cyclophilin D and may play a key role in the permeability transition. J. Biol. Chem. **283**, 26312–26323
22 Detimary, P., Gilon, P., Nenquin, M. and Henquin, J. C. (1994) Two sites of glucose control of insulin release with distinct dependence on the energy state in pancreatic B-cells. Biochem. J. **297**, 455–461
23 Detimary, P., Van den Berghe, G. and Henquin, J. C. (1996) Concentration dependence and time course of the effects of glucose on adenine and guanine nucleotides in mouse pancreatic islets. J. Biol. Chem. **271**, 20559–20565
24 Detimary, P., Gilon, P. and Henquin, J. C. (1998) Interplay between cytoplasmic Ca^{2+} and the ATP/ADP ratio: a feedback control mechanism in mouse pancreatic islets. Biochem. J. **333**, 269–274
25 Katz, L. A., Swain, J. A., Portman, M. A. and Balaban, R. S. (1988) Intracellular pH and inorganic phosphate content of heart *in vivo*: a ^{31}P-NMR study. Am. J. Physiol. **255**, H189–H196
26 Katz, L. A., Swain, J. A., Portman, M. A. and Balaban, R. S. (1989) Relation between phosphate metabolites and oxygen consumption of heart *in vivo*. Am. J. Physiol. **256**, H265–H274
27 Bunger, R., Mallet, R. T. and Hartman, D. A. (1989) Pyruvate-enhanced phosphorylation potential and inotropism in normoxic and postischemic isolated working heart. Near-complete prevention of reperfusion contractile failure. Eur. J. Biochem. **180**, 221–233
28 Ghosh, A., Ronner, P., Cheong, E., Khalid, P. and Matschinsky, F. M. (1991) The role of ATP and free ADP in metabolic coupling during fuel-stimulated insulin release from islet beta-cells in the isolated perfused rat pancreas. J. Biol. Chem. **266**, 22887–22892
29 Erecińska, M., Bryła, J., Michalik, M., Meglasson, M. D. and Nelson, D. (1992) Energy metabolism in islets of Langerhans. Biochim. Biophys. Acta **1101**, 273–295
30 Palmieri, F., Prezioso, G., Quagliariello, E. and Klingenberg, M. (1971) Kinetic study of the dicarboxylate carrier in rat liver mitochondria. Eur. J. Biochem. **22**, 66–74
31 Crompton, M., Palmieri, F., Capano, M. and Quagliariello, E. (1974) The transport of sulphate and sulphite in rat liver mitochondria. Biochem. J. **142**, 127–137
32 Brown, G. C., Lakin-Thomas, P. L. and Brand, M. D. (1990) Control of respiration and oxidative phosphorylation in isolated rat liver cells. Eur. J. Biochem. **192**, 355–362
33 Valdez, L. B., Zaobornyj, T. and Boveris, A. (2006) Mitochondrial metabolic states and membrane potential modulate mtNOS activity. Biochim. Biophys. Acta **1757**, 166–172
34 Dzbek, J. and Korzeniewski, B. (2008) Control over the contribution of the mitochondrial membrane potential ($\Delta\psi$) and proton gradient (ΔpH) to the protonmotive force (Δp). *In silico* studies. J. Biol. Chem. **283**, 33232–33239
35 Martin, D. B. (1995) Bioenergetics. In A Practical Approach (Brown, G. C. and Cooper, C. E., eds), pp. 39–62, Oxford University Press, Oxford
36 Oliveira, G. A. and Kowaltowski, A. J. (2004) Phosphate increases mitochondrial reactive oxygen species release. Free Radic. Res. **38**, 1113–1118
37 Kunz, W., Gellerich, F. N., Schild, L. and Schönfeld, P. (1988) Kinetic limitations in the overall reaction of mitochondrial oxidative phosphorylation accounting for flux-dependent changes in the apparent $\Delta G^{ex}{}_P/\Delta\mu H^+$ ratio. FEBS Lett. **233**, 17–21
38 Nicholls, D. G. (1974) The influence of respiration and ATP hydrolysis on the proton-electrochemical gradient across the inner membrane of rat-liver mitochondria as determined by ion distribution. Eur. J. Biochem. **50**, 305–315
39 Duszyński, J., Bogucka, K. and Wojtczak, L. (1984) Homeostasis of the protonmotive force in phosphorylating mitochondria. Biochim. Biophys. Acta **767**, 540–547

40 Ouhabi, R., Rigoulet, M., Lavie, J. L. and Guérin, B. (1991) Respiration in non-phosphorylating yeast mitochondria. Roles of non-ohmic proton conductance and intrinsic uncoupling. Biochim. Biophys. Acta **1060**, 293–298
41 Czyż, A., Szewczyk, A., Nałcz, M. J. and Wojtczak, L. (1995) The role of mitochondrial potassium fluxes in controlling the protonmotive force in energized mitochondria. Biochem. Biophys. Res. Commun. **210**, 98–104
42 Rigoulet, M., Fraisse, L., Ouhabi, R., Guerin, B., Fontaine, E. and Leverve, X. (1990) Flux-dependent increase in the stoichiometry of charge translocation by mitochondrial ATPase/ATP synthase induced by almitrine. Biochim. Biophys. Acta **1018**, 91–97
43 Hafner, R. P., Brown, G. C. and Brand, M. D. (1990) Analysis of the control of respiration rate, phosphorylation rate, proton leak rate and protonmotive force in isolated mitochondria using the 'top-down' approach of metabolic control theory. Eur. J. Biochem. **188**, 313–319
44 Lambert, A. J. and Brand, M. D. (2004) Superoxide production by NADH:ubiquinone oxidoreductase (complex I) depends on the pH gradient across the mitochondrial inner membrane. Biochem. J. **382**, 511–517
45 Nobes, C. D., Brown, G. C., Olive, P. N. and Brand, M. D. (1990) Non-ohmic proton conductance of the mitochondrial inner membrane in hepatocytes. J. Biol. Chem. **265**, 12903–12909

Received 19 October 2010/21 January 2011; accepted 25 January 2011
Published as BJ Immediate Publication 25 January 2011, doi:10.1042/BJ20101708

Transplant International

Transplant International ISSN 0934-0874

ORIGINAL ARTICLE

Three-dimensional *ex vivo* imaging and analysis of intraportal islet transplants

Hiroyuki Fujimoto,[1] Kentaro Toyoda,[1] Teru Okitsu,[2] Xibao Liu,[1,2] Eri Mukai,[1] Xiaotong Zhuang,[1] Shinji Uemoto,[3] Naoki Mochizuki[4] and Nobuya Inagaki[1,5]

1 Department of Diabetes and Clinical Nutrition, Graduate School of Medicine, Kyoto University, Kyoto, Japan
2 Transplantation Unit, Kyoto University Hospital, Kyoto, Japan
3 Division of Hepato-Pancreato-Biliary Surgery and Transplantation, Department of Surgery, Graduate School of Medicine, Kyoto University, Kyoto, Japan
4 Department of Cell Biology, National Cerebral and Cardiovascular Center Research Institute, Osaka, Japan
5 CREST of Japan Science and Technology Cooperation (JST), Kyoto, Japan

Keywords
allogeneic transplantation, islet transplantation, optical projection tomography, syngeneic transplantation, three-dimensional images.

Correspondence
Nobuya Inagaki, 54 Shogoin Kawahara-cho, Sakyo-ku, Kyoto 606-8507, Japan. Tel.: +81-75-751-3560; fax: +81-75-751-4244; e-mail: inagaki@metab.kuhp.kyoto-u.ac.jp

Conflicts of Interest
All authors have no conflict of interest.

Received: 13 December 2010
Revision requested: 17 January 2011
Accepted: 21 April 2011
Published online: 25 May 2011

doi:10.1111/j.1432-2277.2011.01271.x

Summary

In clinical islet transplantation, because the long-term insulin-independence rate is still poor, a method for detailed analysis of the transplanted islets in the liver after transplantation is required. We have established a novel imaging technique suitable for analysis of transplanted islets in liver using an optical projection tomography (OPT) method. A three-dimensional tomographic image of the transplanted islets in liver was reconstructed. The number of islets transplanted and the number of transplanted islets observed using OPT showed good correlation. The OPT method was used to compare the numbers of transplanted islets in mouse syngeneic and allogeneic transplantation models. Blood glucose concentrations of streptozotocin (STZ)-induced diabetic mice transplanted with syngeneic islets remained normoglycemic and the number of transplanted islets was largely preserved 11 days after transplantation. In mice transplanted with allogeneic islets, hyperglycemia recurred from 7 days after transplantation and the number and the volume of transplanted islets was significantly reduced 11 days after transplantation. These results indicate that OPT imaging and analysis may be a useful tool to quantitatively and sterically evaluation of transplanted islets in liver at the cellular level.

Introduction

Islet transplantation is a promising therapeutic approach for patients with insulin-dependent diabetes mellitus to achieve insulin independence [1,2]. A remarkably high rate of freedom from insulin therapy is achieved in insulin-dependent type 1 diabetic patients after islet transplantation by the Edmonton Protocol [1]. However, it was reported that long-term maintenance of glucose homeostasis without the use of insulin is poor [3]. This decline may be attributed to progressive islet loss as well as to various reactions during and after islet transplantation, including mechanical injury, ischemia, and nonspecific inflammatory reactions [4].

Until now, the total functional volume of islets transplanted intraportally in liver could be monitored only indirectly by measurements such as blood glucose and serum c-peptide levels. Modalities including bioluminescence imaging (BLI) [5–7], magnetic resonance imaging (MRI) [8–11], and positron emission tomography (PET) [12–14] have been used, and transplanted islets were detected by MRI [11] and PET [13] in human. These methods are suitable for *in vivo* examination because they are noninvasive and can be repeated over time. However, islets cannot be evaluated at the cellular level by these methods because the resolution is too low. Conventional immunohistochemical method permit evaluation of beta-cell volume at the subcellular level, but

can only restricted, sliced areas of the sample can be observes. Recently, Hara *et al.* reported subcellular analysis of intact pancreas, but the method can analyze only thin neonatal samples [15]. To investigate engraftment of transplanted islets scattered in solid liver at the subcellular level, another method is required. We have demonstrated an optical projection tomography (OPT) technique for precisely, three-dimensionally evaluating transplanted islets at the cellular level in liver.

Optical projection tomography is a microscopic imaging technique for obtaining three-dimensional, reconstructed images of small biological samples [16]. The principle of OPT is that the light passes through the specimen labeled and cleared for a standard back-projection algorithm to generate a relatively high resolution tomographic image. A three-dimensional image of the specimen is reconstructed using the individual tomographic images. The advantage of OPT is the capability to investigate spatial distribution of such target molecules as RNA and protein without slicing of the target organs and at a higher resolution.

In this report, we show that the number and volume of intraportally transplanted islets in liver can be investigated using OPT analysis. In addition, comparing syngeneic and allogeneic rodent islet transplantation models, we demonstrate that the number and volume of transplanted islets is considerably more decreased in allogeneic islet transplantation than in syngeneic transplantation. Thus, *ex vivo* imaging of intraportal islet transplant using OPT may be a useful tool for evaluation and improvement of islet transplantation outcome.

Materials and methods

Animals

Male C57BL6 Cr Slc mice (Shimizu Laboratory Supplies Co. Ltd, Kyoto, Japan) aged 8–10 weeks were used as recipients and donors and male BALB/c mice (Shimizu Laboratory Supplies Co. Ltd) aged 8 weeks were used as recipients for allogeneic transplantation. All experiments were approved by the Kyoto University Animal Care Committee.

Islet isolation and islet transplantation

Islets were isolated from mouse pancreas using collagenase digestion method [17]; 3–4 ml Hank's Balanced Salt Solution (HBSS) containing 0.5 mg/ml collagenase (Nitta Gelatin, Osaka, Japan) was infused through the common bile duct. The pancreas was dissected and digested at 37 °C for 21 min. Islets were separated from exocrine cells by centrifugation with Ficoll-Conray gradient solution for 10 min. Diabetes was rendered by a single intraperitoneal injection of streptozotocin (STZ) (Nacalai Tesque, Kyoto, Japan), 120 mg/kg body weight, freshly dissolved in 10 mM citrate buffer (pH 4.5). These mice were used as diabetic recipients if the blood glucose concentration was more than 20 mM on two consecutive days. Recipient mice were anesthetized by isoflurane (Forane; Abott, Chicago, IL, USA) during transplantation. Fresh islets in a volume of about 400 μl HBSS were injected into the portal vein and transplanted into the right hepatic lobe as previously reported [18]. For validation of the OPT method, 75, 150 or 300 islets were transplanted into the right hepatic lobe, which was dissected immediately after transplantation. For comparison of syngeneic and allogeneic transplantation, C57BL6 mice (H-2^b) were used as recipients; 300 islets isolated from C57BL6 mice or Balb/c mice (H-2^d) were transplanted, respectively. The blood glucose concentration was determined by glucose meter (Glucocard, Arkley, Japan).

Tissue preparation and immunostaining

Mice with transplanted islets were sacrificed by cervical dislocation. The transplanted right hepatic lobes were dissected clean and immediately immersed for fixation in 4% paraformaldehyde in PBS for 3 h at 4 °C. The fixed samples were washed in PBS and then transferred stepwise to 100% methanol (MeOH) and stored at −20 °C. The immunostaining was performed according to the previous report [19] as follows. The right hepatic lobe was immersed in 15% H_2O_2, 16.7% DMSO solution in MeOH for 24 h to bleach pigmented cells and to reduce auto fluorescence. The liver then was washed in MeOH, which was repeated five times and then kept at −80 °C for at least 1 h before return to room temperature. The organ was rehydrated by Tris Buffered Saline-TritonX (TBST) [0.15 M NaCl (Nacalai Tesque, Kyoto, Japan), 0.1 M Tris (hydroxymethy)aminomethane (Nacalai Tesque, Kyoto, Japan) pH 7.4, and 0.1% Triton X-100 (Nacalai Tesque, Kyoto, Japan)]. TBST containing 10% normal goat serum (Dako Corp., Glostrup, Denmark) and 0.01% sodium azide (Nacalai Tesque, Kyoto, Japan) was used as blocking solution for 24 h. The organ was incubated in insulin antibody (Santa Cruz Biotechnology Inc., Santa Cruz, CA, USA) in 5% DMSO containing blocking solution for 48 h. After washing, Alexa594 goat anti rabbit IgG (Invitrogen, Carlsbad, CA, USA) was used as secondary antibody for 48 h.

Optical projection tomography and image reconstruction

For the observations, the immunostained liver was embedded in 1% agarose gel (low melting point agarose; Sigma Aldrich, St. Louis, MO, USA) to fix the sample.

OPT was performed using an OPT scanner (OPT scanner 3001; Bioptonics, Scotland, UK) according to the manufacturer's instructions [16,19]. The specimens were maintained within the BABB (benzyl alochol/benzyl benzoate 1:2 ratio), rotated to a series of angular positions (0.9° apart) and images were captured at each orientation. High-resolutional tomographic images were reconstructed from raw images by NRecon software (SKYSCAN, Kontich, Belgium). The tomographic images obtained from OPT were reconstructed to three-dimensional form and analyzed by Avizo software (Visualization Science Group, Inc., Burlington, MA, USA). Three-dimensional images of islets and liver were obtained by isosurface treatment. Total volume of all islets was calculated by summation of the selected islets.

Statistical analysis

Data and graph were presented as medians (interquartile range) and statistical analysis was performed with Mann–Whitney's *U*-test. A value of $P < 0.05$ was considered significant.

Results

Observation of transplanted islets in liver by OPT

Transparency of the liver and immunostaining of transplanted islets without sectioning were achieved by the preparation protocols. Figure 1a is a raw OPT image of liver; the insulin-stained transplanted islets are seen as dots in the high magnification image (Fig. 1b, white arrows). One of the tomographic images obtained is shown in Fig. 1c. Vertically reconstructed images are shown in Fig. 1d and e and islets pointed out by arrow and arrowhead in Fig. 1c are located as in Fig. 1d and e, respectively. Some islets appear to be located at the terminal end of the portal vein (Fig. 1c and d) and other islets are located at the wall of the proximal branch of the portal vein (Fig. 1e). Figure 1f is the reconstructed target-specific image of an islet (arrowhead in Fig. 1e) and portal vein. Thus, a three-dimensional image as well as the size and location of transplanted islets in liver can be investigated (Fig. 1g and h and Supplementary movie).

Evaluation of the effectiveness of OPT analysis of transplanted islets in liver

To correlate the number of islets transplanted and the number of islets detected by OPT, we resected and fixed livers immediately after transplantation of a range of numbers of islets. The three-dimensional reconstructed image shows that the number of spots indicating transplanted islets in the right hepatic lobes was increased in accord with the increased dosage (Fig. 2a–c); these numbers are well correlated ($r^2 = 0.9561$) (Fig. 2d). These findings indicate that OPT can be used for quantitative analysis of islets transplanted into liver.

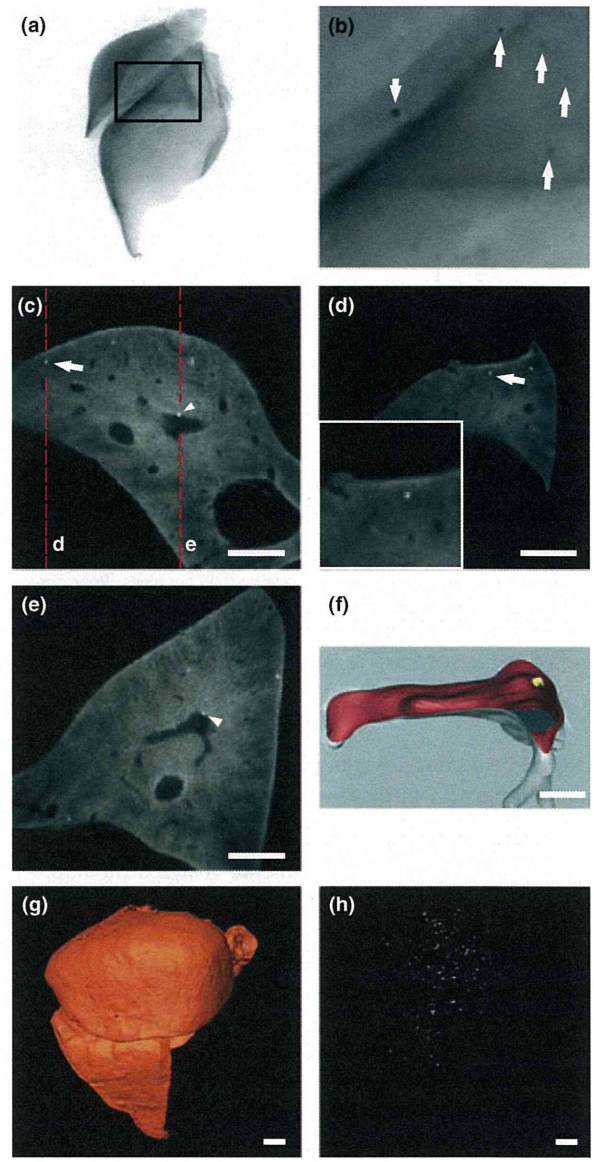

Figure 1 Optical projection tomography (OPT) images of liver containing intraportally transplanted islets. (a) Raw image of islet-transplanted right hepatic lobe, (b) high magnification image [in square of (a)], (c) representative slice image of the transplanted right hepatic lobe; (d and e) vertical slice image of islet with arrow in (c), arrowhead in (c), respectively. (f) Reconstructed three-dimensional image of islet [in (c) and (e), arrowhead] and portal branch. Three-dimensional image of (g) right hepatic lobe; (h) islets (white spots) in liver reconstructed from the same liver sample as (a). Scale bars indicate 1 mm in (c, d, e, g, and h) and 300 μm in (f).

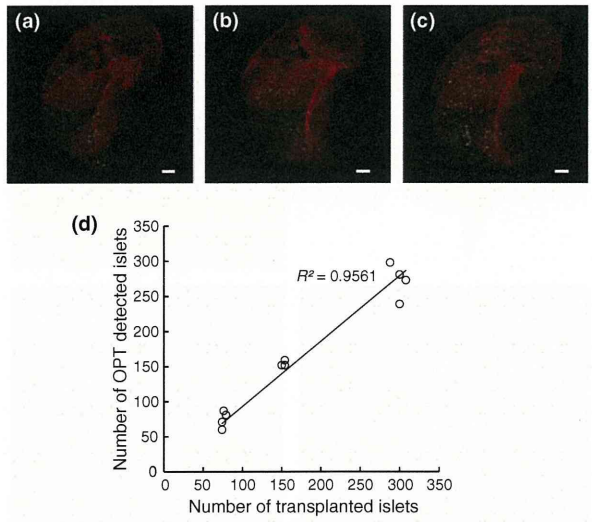

Figure 2 Comparison of the number of islets transplanted with that obtained by optical projection tomography (OPT) analysis. Representative OPT image of recipient liver transplanted with (a) 75, (b) 150, and (c) 300 islets, respectively. (d) Correlation of the number of islets transplanted and OPT-detected islets. Scale bar indicates 1 mm.

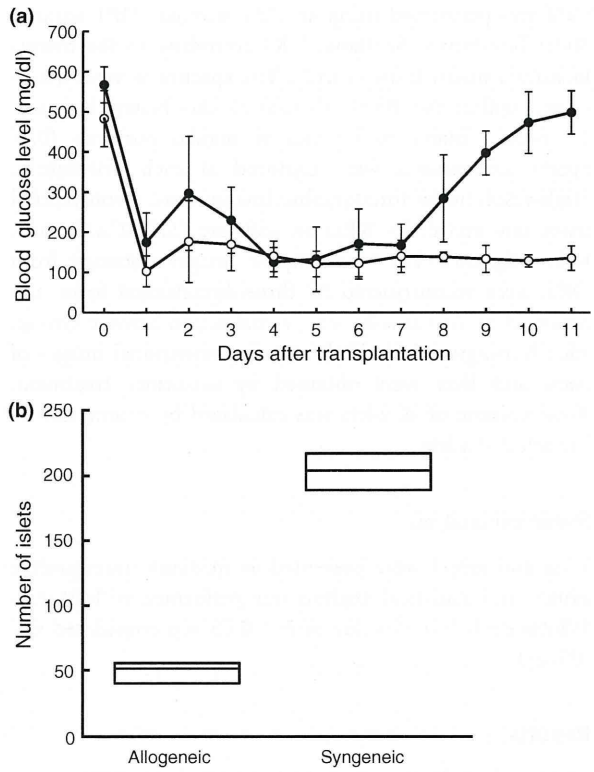

Figure 3 Glycemic level and number of islets of streptozotocin (STZ)-induced diabetic mice after syngeneic and allogeneic islet transplantation. (a) Random blood glucose level of recipients (open circles: syngeneic transplantation, filled circles: allogeneic transplantation). (b) Number of transplanted islets in syngeneic and allogeneic transplantation 11 days after transplantation.

Optical projection tomography analysis of islet grafts under syngeneic and allogeneic conditions

To evaluate the time course of transplanted islets in syngeneic and allogeneic conditions, we analyzed the number and volume of islets intraportally transplanted in liver of STZ-induced diabetic mice. Blood glucose concentrations under both syngeneic and allogeneic conditions were normoglycemic until a week after transplantation. However, blood glucose concentrations under allogeneic conditions thereafter became hyperglycemic, while those under syngeneic conditions remained normoglycemic (Fig. 3a). The islet-containing livers were resected on day 11 for analysis using OPT method. The number of islets in the syngeneic condition was dramatically greater than that in the allogeneic condition [52 (IQR 16.5) vs. 203 (28.5), respectively, $P < 0.05$] (Fig. 3b).

In OPT-detected islets classified by size, the number in each category was significantly greater in syngeneic than in allogeneic conditions and showed a similar histogram pattern (Fig. 4a). Total volume of islets in syngeneic condition was dramatically greater than that in allogeneic condition [8.6 (2.7) vs. 35.3 (10.1) ($\mu m^3 \times 10^6$)], respectively, ($P < 0.05$) (Fig. 4b).

Discussion

In this study, we demonstrate that islets transplanted intraportally in liver can be analyzed at the cellular level using OPT method, which permits three-dimensional analysis of the distribution of the islets in the liver. Comparing syngeneic and allogeneic islet transplantation models, we show by OPT that the volume of transplanted islets differs significantly at the cellular level.

One of main problems in clinical islet transplantation, poor long-term achievement of insulin independence, is primarily attributed to graft loss caused by various stressors upon transplantation [4]. When islets are injected intraportally, each of them is thought to locate at the respective branched end of the portal vein in liver. In modalities such as BLI, MRI, and PET, only PET allows quantification of graft volume, but the resolution is still too low for detailed analysis of the transplanted islets. On the other hand, while the resolution of conventional immunohistochemistry is high, only restricted slices of the engrafted organ can be analyzed using this method.

Optical projection tomography, a newly developed method, is reported to permit analysis of a sample at resolution as high as 5 μm. Recently, Alanentalo *et al.* performed detailed analysis of NOD mice during progression

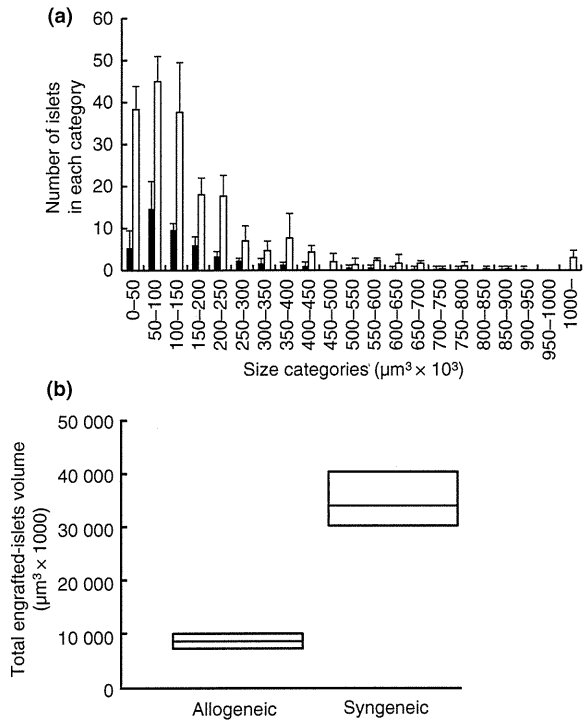

Figure 4 Quantitative analysis of transplanted islets in syngeneic and allogeneic model. (a) Size distribution of transplanted islets. (b) Total volume of transplanted islets in liver obtained using optical projection tomography (OPT) analysis.

of type 1 diabetes and showed that a reduction in volume of native islets in pancreas could be detected and quantified using the OPT method [20]. We have used OPT method for the first time in the intraportal islet transplantation model and confirm the efficacy of this method of islet imaging (Figs 1 and 2).

However, there are several limitations in use of the OPT method. It can be performed only *ex vivo*, and non-invasive, repeated observation is not possible. In this context, PET and MRI are suitable for *in vivo*, repeated monitoring of transplanted islets. In addition, the maximum sample size for analysis using OPT is about 2 cm. The OPT method also is not clinically applicable as it would require a large liver biopsy.

The OPT method is useful for evaluating small organs of small animals such as rodents, as in our present study. Indeed, using rodent islet transplantation models, the OPT method clearly shows quantitative difference of grafts in liver in syngeneic and allogeneic conditions. In this investigation, the OPT method revealed that 83% of the transplanted islets were lost in the allogeneic condition while about 70% were preserved in the syngeneic condition. Moreover, calculated beta-cell volume in the allogeneic condition was significantly reduced to 24.2% of that in the syngeneic condition (Figs 3b and 4b). This remarkable graft loss by allogeneic immune reaction seems not to be related to the size of the islet graft, as there was no difference in size distribution histogram between the two conditions (Fig. 4a). The OPT method also clearly shows the sites where islets adhere and are engrafted in the portal vein. Further investigation is required to determine the effect of islet location on islet engraftment.

In conclusion, we have constructed three-dimensional images of transplanted islets in liver using an OPT method that permits detailed analysis of transplanted islets in liver. This method should be useful for islet transplantation study.

Authorship

HF: designed the study, performed the study, collected the data, analyzed the data, and wrote the paper. KT: designed the study, performed the study, and wrote the paper. TO, SU, and NM: designed the study. XL, EM, and XZ: performed the study. NI: designed the study, wrote the paper.

Funding

This work was supported by a Research Grant from the Ministry of Health, Labour, and Welfare of Japan, and from the Ministry of Education, Culture, Sports, Science, and Technology of Japan, and the Program for Promotion of Fundamental Studies in Health Sciences of the National Institute of Biomedical Innovation (NIBIO), and also by Kyoto University Global COE Program "Center for Frontier Medicine".

Supporting information

Additional Supporting Information may be found in the online version of this article:

Clip S1. Three dimensional image of islets transplanted in liver – Transplanted islets were scattered in liver. This image was reconstructed by software "Avizo".

Please note: Wiley-Blackwell are not responsible for the content or functionality of any supporting materials supplied by the authors. Any queries (other than missing material) should be directed to the corresponding author for the article.

References

1. Shapiro AM, Lakey JR, Ryan EA, *et al.* Islet transplantation in seven patients with type 1 diabetes mellitus using a

glucocorticoid-free immunosuppressive regimen. *N Engl J Med* 2000; **343**: 230.
2. Shapiro AM, Ricordi C, Hering B. Edmonton's islet success has indeed been replicated elsewhere. *Lancet* 2003; **362**: 1242.
3. Ryan EA, Paty BW, Senior PA, *et al.* Five-year follow-up after clinical islet transplantation. *Diabetes* 2005; **54**: 2060.
4. Ricordi C, Strom T. Clinical islet transplantation: advances and immunological challenges. *Nat Rev Immunol* 2004; **4**: 259.
5. Lu Y, Dang H, Middleton B, *et al.* Bioluminescent monitoring of islet graft survival after transplantation. *Mol Ther* 2004; **9**: 428.
6. Fowler M, Virostko J, Chen Z, *et al.* Assessment of pancreatic islet volume after islet transplantation using *in vivo* bioluminescence imaging. *Transplantation* 2005; **79**: 768.
7. Chen X, Zhang X, Larson CS, Baker MS, Kaufman DB. *In vivo* bioluminescence imaging of transplanted islets and early detection of graft rejection. *Transplantation* 2006; **81**: 1421.
8. Evgenov NV, Medarova Z, Guangping D, Bonner-Weir S, Moore A. *In vivo* imaging of islet transplantation. *Nat Med* 2006; **12**: 144.
9. Evgenov NV, Medarova Z, Pratt J, *et al. In vivo* imaging of immune rejection in transplanted pancreatic islets. *Diabetes* 2006; **55**: 2419.
10. Tai JH, Foster P, Rosales A, *et al.* Imaging islets labeled with magnetic nanoparticles at 1.5 Tesla. *Diabetes* 2006; **55**: 2931.
11. Saudek F, Jirák D, Girman P, *et al.* Magnetic resonance imaging of pancreatic islets transplanted into the liver in humans. *Transplantation* 2010; **90**: 1602.
12. Lu Y, Dang H, Middleton B, *et al.* Noninvasive imaging of islet grafts using positron-emission tomography. *Proc Natl Acad Sci USA* 2006; **103**: 11294.
13. Toso C, Zaidi H, Morel P, *et al.* Positron-emission tomography imaging of early events after transplantation of islets of Langerhans. *Transplantation* 2005; **79**: 353.
14. Kim SJ, Doudet DJ, Studenov AR, *et al.* Quantitative micro positron emission tomography (PET) imaging for the *in vivo* determination of pancreatic islet graft survival. *Nat Med* 2006; **12**: 1423.
15. Miller K, Kim A, Kilimnik G, *et al.* Islet formation during the neonatal development in mice. *PLoS ONE* 2009; **4**: e7739.
16. Sharpe J, Ahlgren U, Perry P, *et al.* Optical projection tomography as a tool for 3D microscopy and gene expression studies. *Science* 2002; **296**: 541.
17. Sutton R, Peters M, Mcshane P, Gray DWR, Morris PJ. Isolation of rat pancreatic-islets by ductal injection of collagenase. *Transplantation* 1986; **42**: 689.
18. Yonekawa Y, Okitsu T, Wako K, *et al.* A new mouse model for intraportal islet transplantation with limited hepatic lobe as a graft site. *Transplantation* 2006; **82**: 712.
19. Alanentalo T, Asayesh A, Morrison H, *et al.* Tomographic molecular imaging and 3D quantification within adult mouse organs. *Nat Methods* 2007; **4**: 31.
20. Alanentalo T, Hornblad A, Mayans S, *et al.* Quantification and three-dimensional imaging of the insulitis-induced destruction of β-cells in murine type 1 diabetes. *Diabetes* 2010; **59**: 1756.

Journal of Neuroscience Research

Journal of Neuroscience Research 89:1519–1530 (2011)

Purkinje Cell Protein 4 Positively Regulates Neurite Outgrowth and Neurotransmitter Release

Shin-ichi Harashima,[1]* Yu Wang,[1] Takahiko Horiuchi,[2] Yutaka Seino,[1] and Nobuya Inagaki[1]

[1]Department of Diabetes and Clinical Nutrition, Graduate School of Medicine, Kyoto University, Kyoto, Japan

[2]Department of Medicine and Biosystemic Science, Graduate School of Medical Sciences, Kyushu University, Fukuoka, Japan

Purkinje cell protein 4 (PCP4), also called *brain-specific polypeptide 19* (PEP19), is a neurospecific, small calmodulin-binding protein that binds both calcium-free and calcium-binding calmodulin to regulate the calmodulin-mediated signal. The expression level of this molecule is decreased in the brain in Alzheimer's disease, Huntington's disease, and alcoholism. However, little is known of the function of PCP4 regarding neuronal or neuroendocrine cell differentiation and neurotransmitter release. To address this, we established a PCP4 tetracycline-inducible rat chromaffin cell line, PC12. When PCP4 expression was induced with doxycycline, neurite outgrowth was significantly advanced in the presence of nerve growth factor (NGF) and dibutyryl cAMP, which was inhibited by W-7, a calmodulin inhibitor, and PD98059, an ERK inhibitor. In addition, size of the cell body also was increased by treatment with NGF in the PCP4-induced PC12 cells. Constitutive and potassium-evoked release of acetylcholine and dopamine was increased and apoptosis induced by hydrogen peroxide (H_2O_2) was inhibited in PCP4-induced PC12 cells. On the other hand, knockdown of PCP4 by siRNA transfection decreased neurite outgrowth and dopamine release and increased H_2O_2-induced apoptosis in PC12 cells. These results indicate that PCP4 promotes neuroendocrine cell differentiation and neurotransmitter release by activating calmodulin function.

Key words: PCP4; calmodulin; neuronal cell differentiation; apoptosis; neurodegenerative diseases

Purkinje cell protein 4 (PCP4) is a small calmodulin-binding protein located on human chromosome 21q22 (Cabin et al., 1996; Chen et al., 1996; Hubert and Korenberg, 1997). This molecule is 62 amino acids in length and contains an IQ motif, a binding domain to calmodulin (Gerendasy and Sutcliffe, 1997; Slemmon et al., 2000). Immunohistochemical studies show that PCP4 is expressed predominantly in the cerebellum, especially Purkinje cells, olfactory bulb, piriform cortex, thalamic nuclei, caudate nucleus, putamen, cortex, and hippocampus (Ziai et al., 1988; Sangameswaran et al., 1989). Both mouse and rat PCP4 exhibit 97% homology with human (Ziai et al., 1986; Chen and Orr, 1990; Chen et al., 1996). PCP4 binds calmodulin and modulates calmodulin function. It accelerates the rates of association and dissociation of calcium from the C-domain of free calmodulin and of calmodulin binding to other proteins that regulate calmodulin-mediated signaling pathways (Putkey et al., 2003). For example, overexpression of PCP4 regulates calmodulin-dependent protein kinase II (CaMKII) activity by responding to calcium mobilization in PC12, a rat chromaffin cell line (Johanson et al., 2000). Camstatin, an analogue of PCP4, blocks long-term potentiation and increases calcium extrusion in hippocampal CA1 neurons (Simons et al., 2009).

Expression of PCP4 in the brain is decreased in Huntington's disease and Alzheimer's disease (Utal et al., 1998) and in the prefrontal cortex of alcoholics (Iwamoto et al., 2004). On the other hand, PCP4 is highly expressed in granule cells in dentate gyrus, which are resistant to insult induced by both ischemic damage in Mongolian gerbils (Kirino, 1982) and exposure to excitatory amino acids in Sprague-Dawley rats (Mattson and Kater, 1989). Overexpression of PCP4 in PC12 cells inhibits apoptosis induced by staurosporine and UV irradiation (Erhardt et al., 2000). PCP4 is expressed in ectoderm and neuroectoderm early in development (Thomas et al., 2003). This evidence suggests that PCP4 positively regulates neuronal or neuroendocrine cell differentiation and survival.

*Correspondence to: Shin-ichi Harashima, MD, PhD, Department of Diabetes and Clinical Nutrition, Graduate School of Medicine, Kyoto University, Kyoto 606-8507, Japan. E-mail: harasima@metab.kuhp.kyoto-u.ac.jp

Received 6 November 2010; Revised 8 April 2011; Accepted 11 April 2011

Published online 10 June 2011 in Wiley Online Library (wileyonlinelibrary.com). DOI: 10.1002/jnr.22688

However, other lines of evidence suggest negative regulation. For example, PCP4 is almost 300% increased in the cerebellum of Alzheimer's disease (Slemmon et al., 1994). Ts65Dn, a mouse model of Down syndrome, has a PCP4 gene with trisomy including reduced cerebellar volume, granule cell density, and Purkinje cell density (Olson et al., 2004). In addition, transgenic mice with 2 Mb of human chromosome 21q22.2, in which the PCP4 gene is included (Cabin et al., 1998), show a deficit in learning and memory, with an accompanying decrease in neuronal density (Smith et al., 1997). These lines of evidence suggest that PCP4 negatively regulates neuronal differentiation. The role of PCP4 in neuronal cells remains to be determined.

To address this issue, we established a PCP4-inducible PC12 cell line using a tetracycline-inducible system (TetOn) and examined neuroendocrine cell differentiation, neurotransmitter release, and apoptosis. Here we show that induction of PCP4 in PC12 cells advances neurite outgrowth, enhances acetylcholine and dopamine release, and inhibits hydrogen peroxide (H_2O_2)-induced apoptosis. These results indicate that PCP4 positively regulates neuroendocrine cell differentiation by enhancing calmodulin function.

MATERIALS AND METHODS

Reagents

Doxycycline, pTRE2pur and pTetOn vectors, anti-EGFP antibody (Ab), doxycycline (dox), and TetOn-approved fetal bovine serum (FBS) were purchased from BD Biosciences (Palo Alto, CA); Effectene transfection reagent from Qiagen (Santa Clarita, CA); rabbit anticleaved caspase-3 antibody from Cell Signaling (Danvers, MA); mouse anti-α-tubulin antibody, anticalmodulin antibody, N-(6-aminohexyl)-5-chloro-1-naphthalenesulphonamide (W-7), dibutyryl cAMP (dcAMP), phorbol 12-myristate 13-acetate (PMA), and protein kinase C (PKC) inhibitor from Sigma (St. Louis, MO); NGF 2.5S from Upstate (Chicago, IL); puromycin and geneticin (G418) from Invitrogen (San Diego, CA); and anti-PCP4 antibody from Santa Cruz Biotechnology (Santa Cruz, CA).

Plasmids

The forward and reverse primer sequences for mouse full-length PCP4, 5′-ATGAGTGAGAGACAAAGTGCC-3′ and 5′-GGACTGTGATCCTGACTTTTT-3′ and for EGFP were 5′-ATGGTGAGCAAGGGCGAGGAG-3′ and 5′-CTTGTACAGCTCGTCCATGCC-3′. PCR products were inserted into pTRE2pur vector. All plasmids were sequenced, and no mutations were found.

Establishment of Stable Cell Lines

PC12/TetOn cell lines (BD Biosciences) were maintained in DMEM supplemented with 5% heat-inactivated TetOn-approved FBS, 10% horse serum, 0.2 U/ml bovine insulin, 4 mM L-glutamine, 1.0 mM sodium pyruvate, 0.2 mg/ml G418, 100 U/ml penicillin, and 100 μg/ml streptomycin at 37°C in 90% air and 10% CO_2. Both pTRE2-pur/EGFP and pTRE2pur/PCP4-EGFP were introduced into PC12/TetOn cells using Effectene transfection reagent, and a stable, single clone was obtained by limiting dilution with 0.3 mg/ml G418 and 3 μg/ml puromycin. For induction of EGFP and PCP4-EGFP, PC12/TetOn cells were cultured with 1 μg/ml dox for the time indicated, and each molecule was detected by Western blot analysis.

Western Blot

Cells were washed twice with PBS, detached from plates with trypsin-EDTA, collected, washed two more times with ice-cold PBS, and then sonicated in lysis buffer. Twenty micrograms of total protein were resolved by SDS-PAGE on 4–12% acrylamide gels (Invitrogen) and transferred to PVDF membranes (Invitrogen), followed by immunoblotting with antibodies to EGFP, α-tubulin, calmodulin, PCP4, and cleaved caspase-3.

Immunoprecipitation

EGFP-transfected and PCP4-EGFP-transfected PC12/TetOn cells cultured with or without 1 μg/ml doxycycline were washed twice with PBS, and immunoprecipitation was performed with protein G immunoprecipitation kit (Sigma). Cell lysates were incubated with antibodies to EGFP or calmodulin or IgG (control) overnight at 4°C, followed by Western blot to detect calmodulin or PCP4-EGFP.

Measurement of Acetylcholine Release

EGFP- and PCP4-EGFP-induced PC12/TetOn cells (1.0×10^5) were seeded in 24-cell culture plates coated with poly-L-lysine and incubated in DMEM for 3 days with 1 μg/ml dox and 50 ng/ml NGF. Cells were washed three times with Krebs-Ringer's solution bicarbonate Hepes (KRBH) buffer (140 mM NaCl, 4.7 mM KCl, 2.5 mM $CaCl_2$, 1.2 mM $MgSO_4$, 1.2 mM KH_2PO_4, 11 mM glucose, and 20 mM Hepes at pH 7.4). The attached cells were incubated at 37°C for 60 min in KRBH with 4.7 mM K^+ and then incubated for 10 min in KRBH including 4.7 mM or 25 mM K^+. Supernatants were collected and ACh concentration was measured by Amplex red ACh/ACh elastase assay kit (Invitrogen, Carlsbad, CA).

Measurement of Uptake and Release of [^{3}H]Dopamine

EGFP- and PCP4-EGFP-induced PC12/TetOn cells (1.0×10^5) were seeded in 24-cell culture plates coated with poly-L-lysine and incubated in DMEM for 3 days with 1 μg/ml dox and 50 ng/ml NGF. For uptake assays, cells were washed three times with KRBH and incubated with [^{3}H]dopamine (0.5 μCi) for 10 min at 37°C. After removal of excess [^{3}H]dopamine, the cells were washed three times rapidly with an ice-cold KRBH buffer and extracted with NaOH, and radioactivity was measured with a liquid scintillation counter. For the release assays, cells were incubated with [^{3}H]dopamine for 2 hr and stimulated with 4.7 mM K^+ or 25 mM K^+ for 6 min at 37°C. Supernatants were collected and rapidly centrifuged at 10,000*g* for 20 sec at 4°C, and the radioactivity was then measured with a liquid scintillation counter.

siRNA and Transfection

PCP4 siRNA and nonsilencing (scramble) siRNA were purchased from Applied Biosystems (Foster City, CA). In total, 1×10^5 nontransfected PC12 cells were seeded into six-well culture plates coated with poly-L-lysine (Sigma) and cultured for 24 hr. The cells then were transfected with 2 μg PCP4 siRNA or 2 μg scramble siRNA by Lipofectamine 2000 (Invitrogen). Forty-eight hours later, the cells were used for the following experiments.

Neurite Outgrowth Quantification

Neurite outgrowth was quantified with a neurite outgrowth quantification assay kit (Chemicon, Orlando, FL). The chamber membrane was placed into a well of a 24-well culture plate containing 500 μl DMEM with 50 ng/ml NGF or 0.5 mM dcAMP or 10 nM to 1 μM PMA, and 5.0×10^3 cells precultured for 48 hr in serum-free conditioning media with 1 μg/ml dox were added on top of the membrane and incubated for the indicated periods at 37°C. Neurites were stained with neurite stain solution for 10 min at room temperature, and cell bodies were removed from the surface of the upper membrane by wiping with a cotton swab. For quantification, the underside of the membrane was incubated in 200 μl of neurite stain extraction buffer for 5 min at 37°C and quantified by spectrophotometer at 562 nm.

Measurement of Neurite Outgrowth by Confocal Microscopy

EGFP- or PCP4-EGFP-induced PCP4/TetOn cells treated with or without 50 ng/ml NGF or 0.5 mM dcAMP or 100 nM PMA for the indicated periods were fixed in PBS containing freshly prepared 4% paraformaldehyde for 20 min, and only individual cells in a total of 50 cells were used for measurement using transmitted light images captured with a Leica confocal microscope (TSC STED, Bannockburn, IL) and Image J 1.30 software. For measurement of neurite outgrowth, the segmented line tool of Image J 1.30 was used to calculate the longest neurite length of a cell. For measurement of size of cell body, color images were converted to gray scale, and the area of cell bodies was automatically calculated by the image processing program.

DNA Fragmentation

After incubation with 1 μg/ml dox for 48 hr, EGFP- and PCP4-EGFP-induced PC12/TetOn cells were cultured with 0.2 or 1.0 mM H_2O_2 for 24 hr. Cells were collected, and both fragmented and high-molecular-weight DNA were extracted from the cells with a Suicide-Track DNA ladder isolation kit (EMD Chemicals), and the extracts were applied to a 1.5% agarose gel.

Detection of Apoptotic Cells

PC12 cells or PC12/TetOn cells were cultured with 0.2 or 1.0 mM H_2O_2 for 24 hr, then detached from the plates with trypsin-EDTA and washed with PBS. Apoptotic cells were detected by annexin-V-Alexa 568 and BOBO-1 staining kit (Roche), and 200 cells were analyzed by fluorescent microscopy (BZ-8100; Keyence). Only annexin-V-positive and BOBO-1-netagtive apoptotic cells were counted, and the ratio of H_2O_2-induced apoptotic cells is shown compared with that of nontreated cells. Caspase-3 activity was detected by Western blot analysis using an anticleaved caspase-3 antibody.

Statistical Analysis

All data are expressed as mean ± SE. Student's *t*-test was used to determine statistical significance.

RESULTS

Establishment of PCP4-EGFP-Inducible PC12/TetOn Cells

We established PCP4-inducible PC12 cells with the TetOn system (PC12/TetOn cells). The full length of mouse PCP4 fused with EGFP at the C-terminus (PCP4-EGFP; Fig. 1A) or EGFP alone (control) was transfected into PC12/TetOn cells, and a stable cell line was cloned with genecitin (G418) and puromycin selection and limiting dilution. Western blot analysis with an antibody directed toward EGFP showed that EGFP expression was gradually increased in a time-dependent manner by treatment with 1 μg/ml dox compared with that with PBS and reached about a 3.5-fold increase at 48 hr (Fig. 1B,C). PCP4-EGFP expression also was increased by dox in a time-dependent manner compared with that treated with PBS and reached about a fourfold increase at 48 hr (Fig. 1D,E). Fluorescent micrographs showed that EGFP and PCP4-EGFP-induced PC12 cells emitted stronger intensity of green fluorescence by treatment with dox for 48 hr (Fig. 1F).

PCP4 Interacts With Calmodulin and Increases ERK Phosphorylation

PCP4 has been reported to bind calmodulin (Gerendasy and Sutcliffe, 1997; Slemmon et al., 2000), so we examined the interaction between PCP4-EGFP and calmodulin by immunoprecipitation. When PCP4 was pulled down with an anti-EGFP antibody in EGFP- or PCP4-EGFP-induced PC12/TetOn cells, Western blot analysis using an anticalmodulin antibody showed that calmodulin interacted with PCP4-EGFP but not with EGFP (Fig. 2A). In contrast, PCP4-EGFP but not EGFP was coimmunoprecipitated with calmodulin using an anticalmodulin antibody (Fig. 2B). These results demonstrate that PCP4-EGFP binds to calmodulin. We therefore wanted to determine whether PCP4-EGFP activates calmodulin function. Because extracellular signal-regulated kinase (ERK) is phosphorylated by nerve growth factor (NGF) via a calmodulin signaling pathway in PC12 cells (Agell et al., 2002), EGFP- and PCP4-EGFP-induced PC12/TetOn cells were treated with 50 ng/ml NGF for 30 min and ERK phosphorylation was detected by Western blot analysis. In EGFP-induced PC12/TetOn cells, ERK phosphorylation was not enhanced by the treatment with dox, whereas 50 μM W-7, a calmodulin inhibitor, significantly inhibited ERK phosphorylation (Fig. 2C,D). On the other hand,

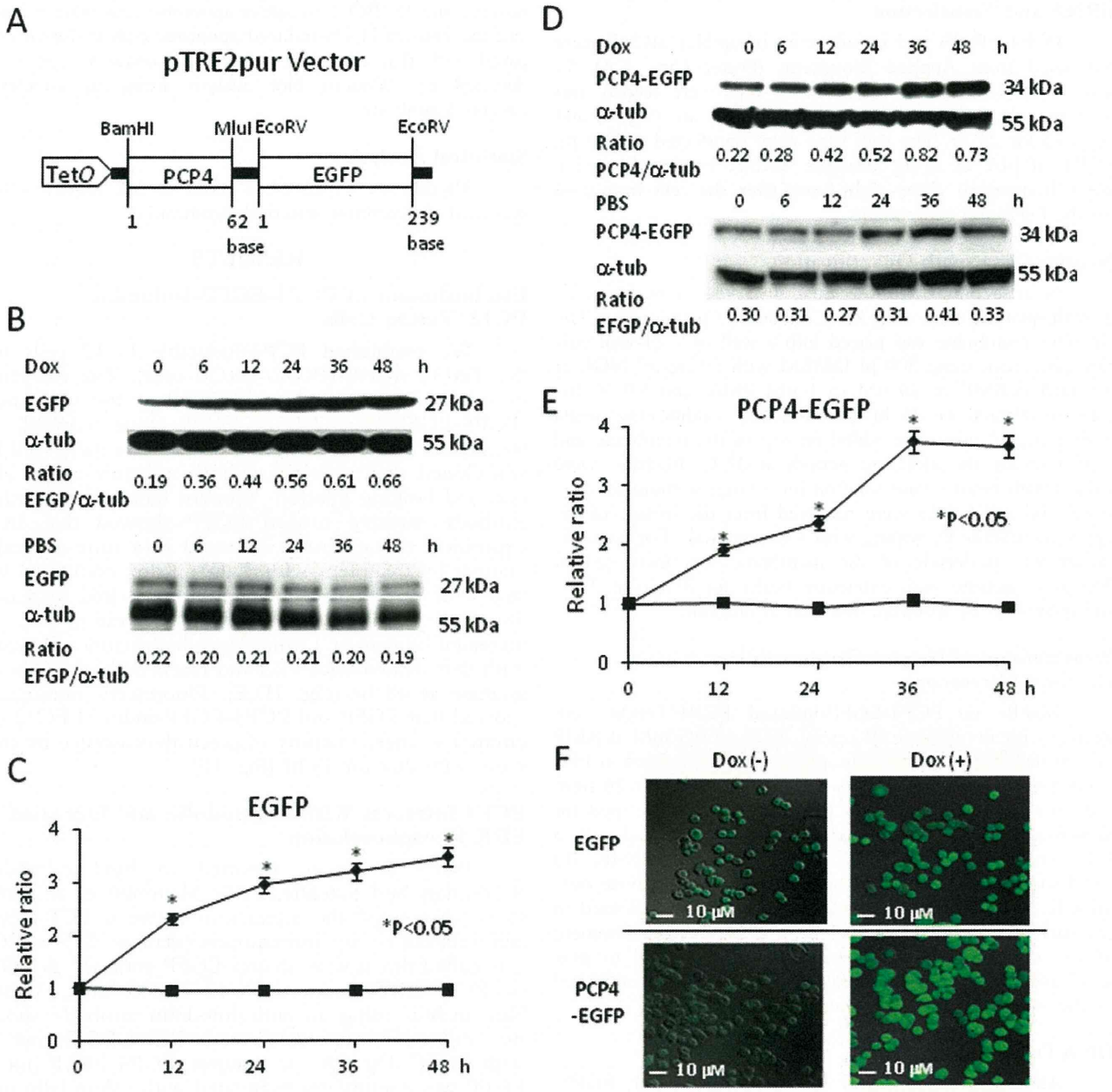

Fig. 1. Establishment of PCP4-EGFP-inducible PC12/TetOn cells. **A:** PCP4-EGFP-inducible vector construct. **B,C:** EGFP induction by treatment with 1 μg/ml doxycycline (dox). Western blot analysis shows time course of induction of EGFP in PC12/TetOn cells (B). Graphs show relative ratio of EGFP vs. α-tubulin (C). **D,E:** PCP4-EGFP induction by treatment with 1 μg/ml dox. Western blot analysis shows time course of induction of PCP4-EGFP in PC12/TetOn cells (D). Graphs show relative ratio of PCP4-EGFP vs. α-tubulin (E). **F:** Fluorescent micrographs shows representative images of EGFP- or PCP4-EGFP-induced PC12/TetOn cells after treatment with or without 1 μg/ml dox for 48 hr. Images are representative of three independent experiments. Data are means ± SE of three independent experiments. $*P < 0.05$. α-tub, α-Tubulin.

ERK phosphorylation was increased about twofold in PCP4-EGFP-induced PC12/TetOn cell but was significantly inhibited by 50 μM W-7 (Fig. 2E,F). These data indicate that PCP4-EGFP increases ERK phosphorylation by activating calmodulin function.

PCP4 Promotes Neurite Outgrowth and Increases Size of Cell Body in PC12 Cells

ERK phosphorylation is important for PC12 cell differentiation (Vaudry et al., 2002), so we examined neurite outgrowth in PCP4-EGFP-induced PC12/

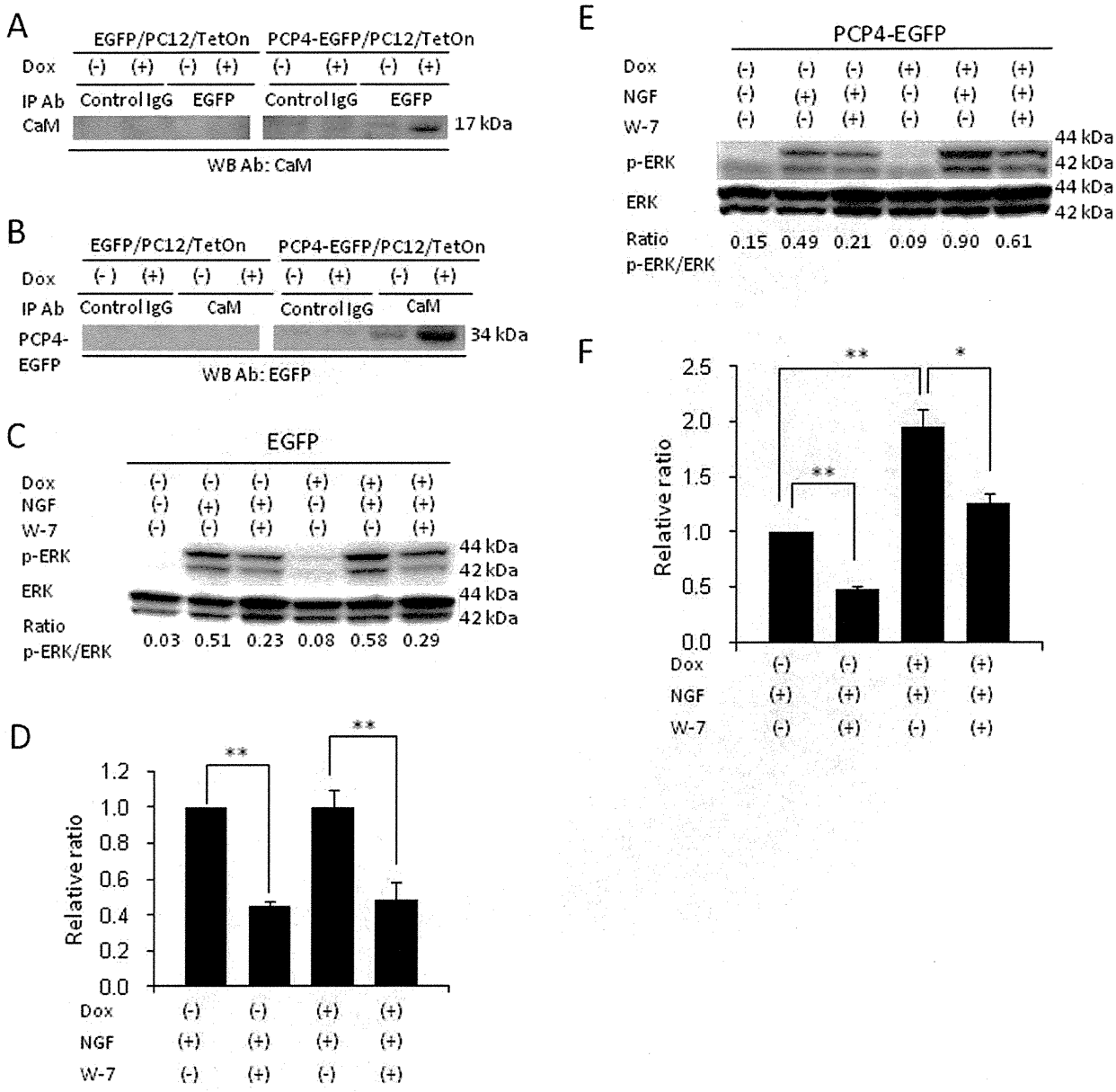

Fig. 2. PCP4 binds to calmodulin and increases ERK phosphorylation. **A,B:** Immunoprecipitation of PCP4-EGFP and calmodulin after treatment with 1 μg/ml doxycycline (dox) for 48 hr. Calmodulin was immunoprecipitated with PCP4-EGFP with an anti-EGFP antibody (A) or PCP4-EGFP was pulled down with calmodulin using an anticalmodulin antibody (B) in PCP4-EGFP-induced PC12/TetOn cells. **C,D:** ERK phosphorylation by treatment with NGF in EGFP-induced PC12/TetOn cells. After induction with dox for 48 hr, cells were incubated with 50 ng/ml NGF in the presence or absence of 50 μM W-7 for 30 min, and ERK phosphorylation was detected by Western blot analysis (C). Graphs show relative ratio of phosphorylated ERK vs. total ERK (D). **E,F:** ERK phosphorylation by treatment with NGF in PCP4-EGFP-induced PC12/TetOn cells. After induction with dox for 48 hr, cells were incubated with 50 ng/ml NGF in the presence or absence of 50 μM W-7 for 30 min, and ERK phosphorylation was detected by Western blot analysis (E). Graphs show relative ratio of phosphorylated ERK vs. total ERK (F). Images are representative of three independent experiments. Data are means ± SE of three independent experiments. $\star P < 0.05$, $\star\star P < 0.01$. IP, immunoprecipitation; WB, Western blot; Dox, doxycycline; NGF, nerve growth factor.

TetOn cells. PCP4-EGFP- and EGFP-inducible PC12/TetOn cells were treated with 1 μg/ml dox for 48 hr and cultured for an additional 48 hr in the presence of 50 ng/ml NGF and 1 μg/ml dox. Fluorescent micrographs showed much greater extension of neurite outgrowth in PCP4-EGFP-induced PC12/TetOn cells than